Review | Open Access

Iontronics

Cui *et al. Iontronics* **2026**, *2*, 26 **DOI:**10.20517/iontronics.2026.17

2D organic framework membranes: extending functions in natural ion channels to scalable nanofluidic applications

Hongyu Cui[1,2,3], Yu Ji[1], Ke Chen[2], Wenzhe Zhou[1], Qiaowei Lin[2], Zhuocheng Yin[1], Li Lin[4,5], Da-Wei Wang[2,3,*], Pengzhan Sun[1,*]

Keywords:
2D organic framework, nanofluidics, nanopore, ion transport

Citation: Cui, H.; Ji, Y.; Chen, K.; Zhou, W.; Lin, Q.; Yin, Z.; Lin, L.; Wang, D. W.; Sun, P. 2D organic framework membranes: extending functions in natural ion channels to scalable nanofluidic applications. *Iontronics* **2026**, *2*, 26. https://dx.doi.org/10.20517/iontronics.2026.17

Received: 24 May 2026 **First Decision:** 18 Jun 2026 **Revised:** 8 Jul 2026 **Accepted:** 10 Jul 2026 **Published:** 7 Aug 2026

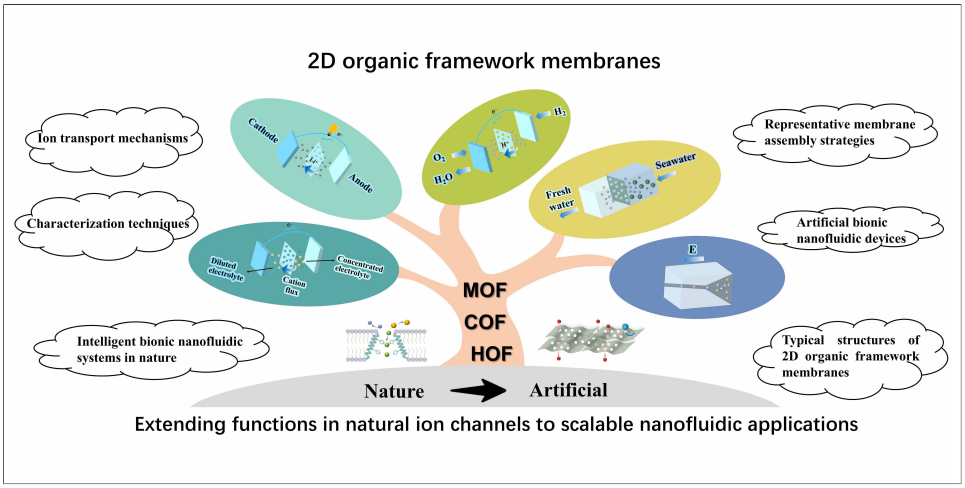

Abstract

Precise regulation of ion transport across nanoscale channels is fundamental to many functions in biological systems, which in turn offers a blueprint for the design of advanced artificial nanofluidic systems targeted for energy storage, energy conversion, water purification, and many other applications. Two-dimensional (2D) organic framework membranes have emerged as a new platform for controllable ion transport. These membranes provide intrinsic periodicity, controllable sub-nanometer pore structures, and adjustable chemical environments and hence, could potentially reproduce the ionic machinery of living organisms. More importantly, the scalability of membrane-based systems is long sought after for addressing critical challenges faced by many energy, environment and other areas. In this review, we discuss the fundamental mechanisms and

[1]Institute of Applied Physics and Materials Engineering, University of Macau, Macau SAR 999078, China.
[2]Faculty of Materials Science and Energy Engineering, Shenzhen University of Advanced Technology, Shenzhen 518107, Guangdong, China.
[3]Institute of Technology for Carbon Neutrality, Shenzhen Institute of Advanced Technology, Chinese Academy of Sciences, Shenzhen 518055, Guangdong, China
[4]School of Materials Science and Engineering, Peking University, Beijing 100871, China.
[5]Beijing Graphene Institute, Beijing 100095, China.

[*]**Correspondence to:** Prof. Pengzhan Sun, Institute of Applied Physics and Materials Engineering, University of Macau, Macau SAR 999078, China. E-mail: pengzhansun@um.edu.mo; Prof. Da-Wei Wang, Faculty of Materials Science and Energy Engineering, Shenzhen University of Advanced Technology, Shenzhen 518107, Guangdong, China; Institute of Technology for Carbon Neutrality, Shenzhen Institute of Advanced Technology, Chinese Academy of Sciences, Shenzhen 518055, Guangdong, China. E-mail: wangdawei@suat-sz.edu.cn

experimental measurements for nanofluidic ion transport, fabrication of 2D organic framework membranes and potential applications. Finally, we assess the key challenges and provide an outlook on the future roadmap for 2D organic framework membranes in next-generation nanofluidics.

INTRODUCTION

Nature performs many exquisite tasks with ions and fluids at small scales with remarkable efficiency[1]. A representative example is biological ion channels, which are ubiquitous in living organisms. They are membrane proteins assembled from polypeptides[2,3] and exhibit precisely defined pore morphologies decorated with a high density of functional groups. This unique structure combination creates a confined environment with specific polarity, which energetically and entropically favors the selective partitioning of target ions. Consequently, these biological ion channels enable ultra-rapid transport of specific ions (approximately 10^6-10^8 ions per second per channel) with exceptional selectivity[4,5]. This efficient transmembrane ion transport is essential for key physiological processes, including the regulation of electrical potentials, energy production and storage, and signal transmission and processing[6].

Nanofluidics[7] aims to mimic the properties and functions of biological ion channels using artificial devices with nanometer or sub-nanometer pores and tunable pore wall chemistry. So far, the fundamental understanding of molecular and ionic transport through (sub) nanopores exhibits great potential in applications demanding highly efficient ionic transport, including desalination, osmotic energy conversion, Li-batteries, and proton conductors[7-9]. However, the real applications in these fields require moving beyond the passive response of individual nanochannels toward integrated devices or membranes that incorporate high-density channels. Also, intelligent membranes enabling stimulus-responsive ion transport that can be dynamically controlled by external triggers such as pH, electric fields, or light[10] are highly desired. To fabricate such membranes, one of the feasible strategies is to cast or vacuum-filtrate colloidal suspensions of exfoliated nanosheets, such as graphene oxide, MoS_2, and clay[11-13], so that 2D and horizontally aligned nanochannels can be formed within the interlayer space of the resulting lamellar membranes. With these membranes formed from stacked and overlapped 2D nanosheets, the selectivity toward the permeating species can be finely tuned by controlling interlayer spacing and surface chemistry[14,15]. Despite the ease of fabrication, ion transport in these membranes is hindered by long and tortuous lateral pathways, resulting in limited ionic mobility and transmembrane permeance. While vertically realigning the lamellae would shorten the transport route and therefore improve the permeance, the scalable fabrication of such vertically oriented architectures remains elusive[16]. The 2025 Nobel Prize in Chemistry, awarded to three scientists for their work on metal-organic frameworks (MOFs), not only highlights the profound scientific value of MOFs but also brings the entire field of crystalline porous materials to public attention[17]. Over the past decade, 2D organic framework membranes have garnered significant attention for nanofluidic applications due to their ordered pore structures, designer species-to-species selectivity, and large pore volumes enabling high ionic flux[18]. Key classes include 2D MOFs, 2D covalent organic frameworks (COFs), and 2D hydrogen-bonded organic frameworks (HOFs)[19]. These materials comprise nanosheets with intrinsically uniform pore structures, featuring tunable pore windows and cage architectures. Therefore, they could serve as good building blocks for constructing crystalline and porous membranes.

Herein, the state-of-the-art development of 2D organic framework membranes is reviewed [Figure 1]. We begin with a concise overview of intelligent bionic nanofluidic systems in nature and their artificial counterparts. Next, we outline the key characterization techniques and theoretical frameworks that could measure and understand the confined ion transport in bionic nanochannels. We then overview a few representative examples of 2D organic framework membranes, with an emphasis on their rich chemical diversity, structural tunability, and versatile topological features. Following a discussion on the underlying

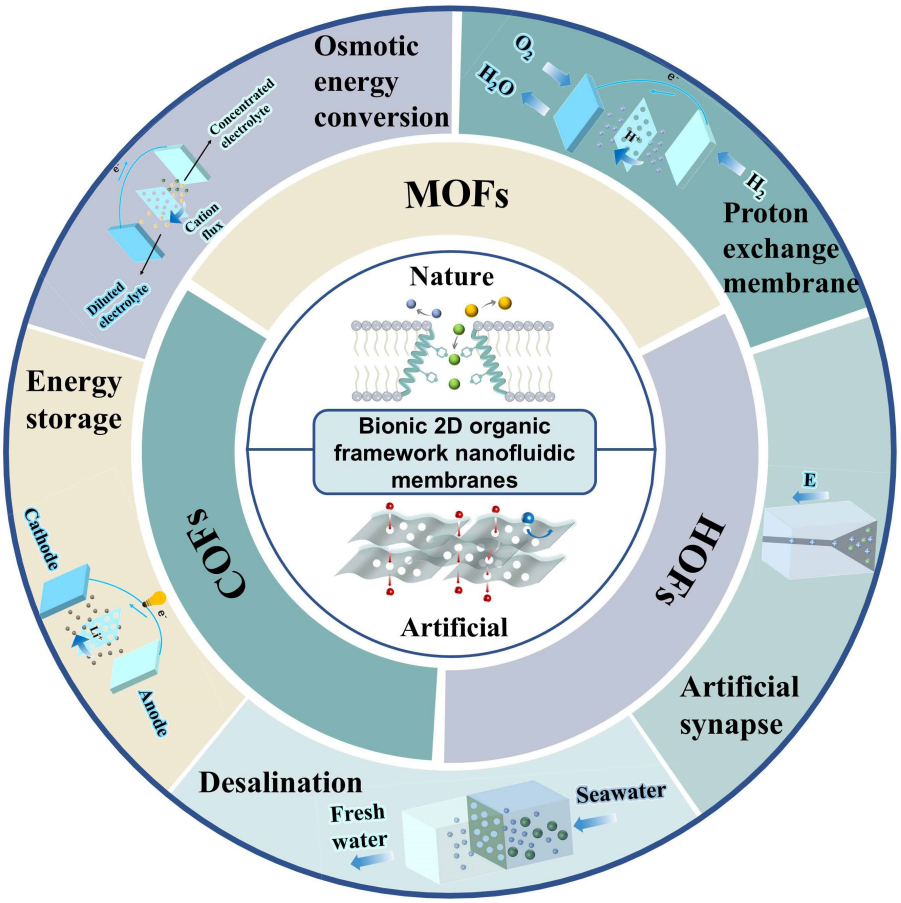

Figure 1. Outline of the main topics: bionic 2D organic framework membranes for nanofluidic applications. MOF: Metal-organic framework; COF: covalent organic framework; HOF: hydrogen-bonded organic framework.

transport mechanisms, we summarize strategies for scaling up the 2D organic framework building blocks toward macroscopic membranes, and discuss their potential in addressing key challenges in nanofluidic applications requiring highly efficient ion transport. Finally, we conclude with a perspective on the development of bionic 2D organic framework membranes.

FROM NATURAL PROTOTYPES TO ARTIFICIAL ARCHITECTURES

Biological ion channels represent the gold standard in nanofluidics, achieving a seemingly paradoxical combination of ultra-high selectivity and near-diffusion-limit throughput. For example, potassium ion (K^+) channels discriminate against sodium (Na^+) ions by a factor exceeding 10^3, despite their identical charge and similar hydrated radii[5]. Moreover, these channels maintain ion transport fluxes ~ 10^8 ions per second, near the theoretical diffusion limit and significantly surpassing the performance of current synthetic ion-selective materials[20]. However, replicating this synergy of precision and efficiency in artificial systems remains a paramount challenge in membrane science.

Intelligent bionic nanofluidic systems in nature

After more than 4.6 billion years of evolution, nature has designed a series of intelligent nanofluidic systems. Embedded through cell membranes, biological protein channels act as exquisite regulators of metabolite transport and are indispensable to life[21]. These structures overcome substantial energy barriers to facilitate long-distance mass transport[22]. Among them, ion channels represent a paradigm of high selectivity, enabling passive yet specific ion permeation. Typical examples include monovalent cation channels such as

the TrkH K^+ transporter, which stabilizes the resting membrane potential, and the Nav1.4-β1 voltage-gated Na^+ channel, which is responsible for the high-voltage discharges in electric eels[23]. These channels are pivotal in modulating membrane excitability and generating bioelectrical signals. In addition to voltage gating, ligand- and stimulus-responsive mechanisms are equally critical. For instance, calcium-activated chloride channels (CaCCs) open upon elevated intracellular Ca^{2+}, driving Cl^- fluxes that regulate neuronal excitability, muscle contraction, and secretory functions[24]. Similarly, the plant mechanosensitive channel MSL10 transduces mechanical stimuli, such as touch, directly into electrical signals[25]. Divalent ion channels also play critical roles. For example, the voltage-gated calcium channel Cav1.2 mediates Ca^{2+} flux to regulate processes including blood coagulation and muscle contraction, often in coordination with calcium-sensing proteins such as troponin C and calmodulin[26]. Copper homeostasis relies on COPT (Copper Transporter) proteins, which facilitate high-affinity Cu^+ uptake across the plasma membrane, influencing oxidative stress response and iron metabolism[27]. The CorA channel found in bacterial cells functions as the primary Mg^{2+} transporter[28]. Note that one of the unbeatable advantages of biological systems compared to their artificial counterparts is the exceptional energy efficiency[29]. In this context, a striking example is the human brain, which accomplishes sophisticated perception and computational tasks with an estimated power consumption of only 20 W. This remarkable efficiency largely stems from the nonlinear, history-dependent gating mechanisms of ion channel proteins[29]. Such highly efficient biological transport and signaling mechanisms offer fundamental design principles for developing bionic nanofluidic systems.

Artificial bionic nanofluidic devices

The modern understanding of ion channels could trace back to the seminal 1952 work of Hodgkin and Huxley on the action potential in the squid giant axon, which laid the foundation for decades of research in this field [Figure 2]. Their theoretical framework proposed that electrical excitability arises from dynamic changes in the axon membrane's permeability to Na^+ and K^+[30,31]. In the following two decades, Armstrong and Hille utilized electrophysiological methods to demonstrate that Na^+ and K^+ ions pass through cell membranes via separate protein channels. Their work introduced fundamental concepts such as selectivity filters for ion discrimination and gating mechanisms for permeability control[32]. The patch-clamp recording technique, pioneered by Neher and Sakmann in 1971, enabled the detection of electrical signals from individual ion channels, which is an achievement recognized with the Nobel Prize in Physiology or Medicine in 1991[32]. Another breakthrough came in 1998 when MacKinnon resolved the atomic structure of a potassium channel and therefore elucidated the molecular basis of K^+ conduction[33]. The described fundamental understandings gained from biological systems have inspired the development of diverse artificial platforms capable of transmembrane transport of various species and through various mechanisms. The first artificial ion channels were reported in 1982[34]. Later, in the early 2000s, research on regulating ion transport focused primarily on one-dimensional (1D) nanostructures. These early nanofluidic devices typically feature single or a few channels and were fabricated from conventional cleanroom materials like silicon and glass wafers[35].

Understanding molecular transport in confined environments is crucial for understanding the working mechanism of biological systems and also, for the development of technologies for applications such as separation, sensing, and drug delivery. Since 2000, advances in micro-/nanofabrication and nanoscale imaging techniques have propelled nanofluidics, a field dedicated to exploring fluid transport in spaces of 1-100 nm in size, which has become a rapidly expanding global research frontier[36]. With the advent of graphene, the nanofluidics community has sought to use graphene and other 2D inorganic materials for membrane fabrication[37]. To this end, two strategies are generally employed: (1) to perforate (sub) nanopores in the 2D matrix so that combined high selectivity and flow rates are expected from the atomic thickness and the precisely defined nanopores[38,39]; (2) to assemble the 2D flakes into lamellar membranes and take advantage of the ion-surface interactions[40,41]. On the other hand, inspired by 2D inorganic nanomaterials,

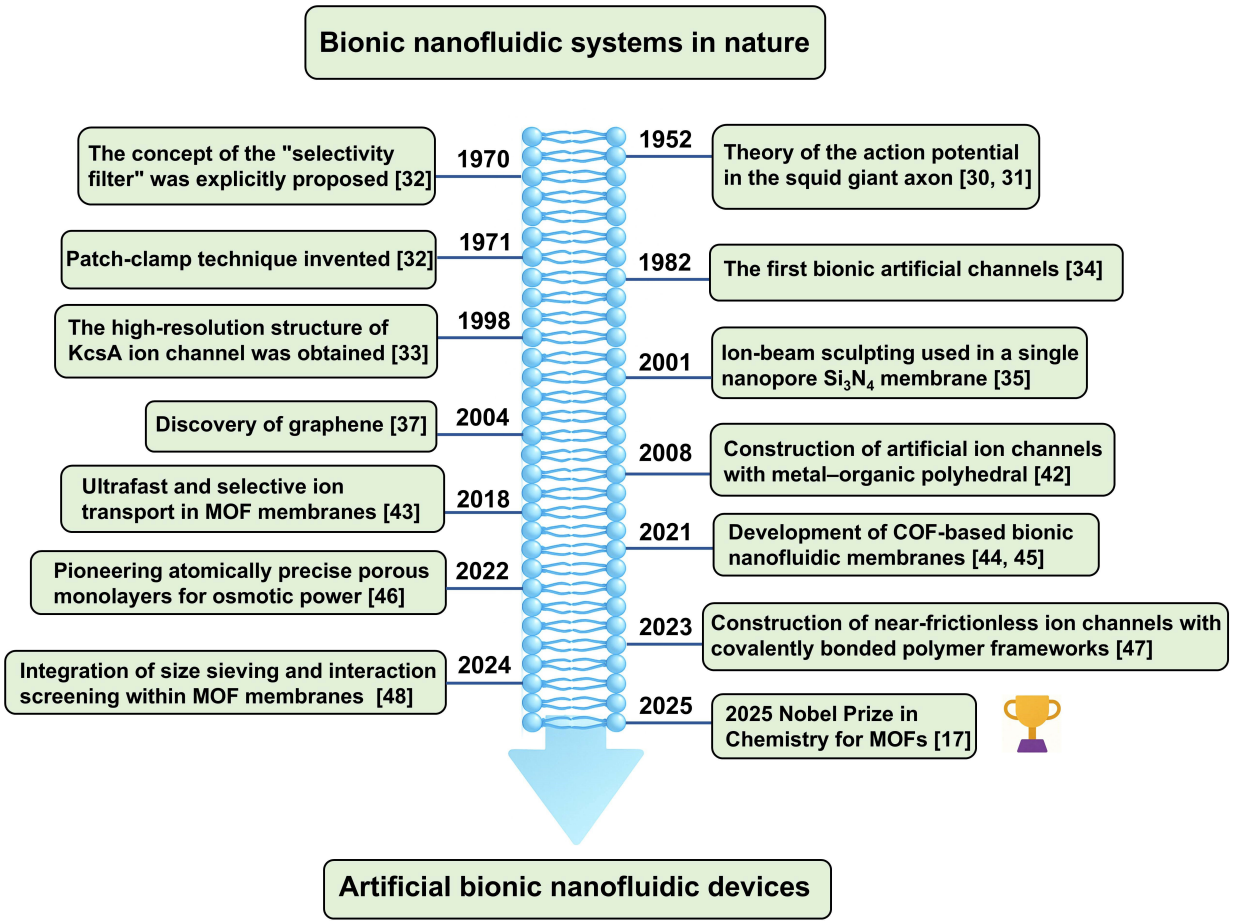

Figure 2. Timeline of advances from natural nanofluidic systems to artificial architectures. MOF: Metal-organic framework; COF: covalent organic framework.

researchers have also pursued the synthesis of organic-based porous materials with tailored pore structures[42].

Recent progress in organic framework membranes has enabled highly precise molecular regulation. Sub-nanometer pores in MOFs can drive monovalent ion separation through dehydration, overcoming the standard permeability-selectivity limits[43]. Following a similar structure, COFs utilize engineered pore environments to replicate biological functions, such as thermal sensation and targeted lithium extraction[44,45]. These organic framework materials have seen rapid development and widespread application in recent years. For instance, COF monolayers with atomically precise pores were introduced in 2022 for osmotic power generation, utilizing their high pore density and tunable surface charges[46]. The following year, rigid covalent triazine framework membranes achieved near-frictionless ion transport through optimized pore-wall interactions, enabling fast-charging aqueous flow batteries[47]. By 2024, confining crown ethers within MOF cavities integrated size sieving and interaction screening to achieve complete ion dehydration and rapid separation[48]. The foundational importance of these architectures was highlighted when the 2025 Nobel Prize in Chemistry was awarded for the development of MOFs[17]. Spurred by continuous advances in organic framework material design and bionic nanofluidics, diverse organic framework membranes are now driving the rapid development of iontronics.

Table 1. Comparison of ion transport functions between natural ion channels and 2D organic framework membranes

Function	Natural ion channels	2D organic framework membranes
Ion selectivity	KcsA channel: K^+/Na^+ selectivity (> 1,000)[51].	1D MOF-in-2D COF membrane: K^+/Na^+ selectivity (82.52)[52]
Ultrafast transport	KcsA channel: High flux of 10^7 ~ 10^8 ions•s^{-1}[20]	Quaternary ammonium-group-functionalized COF membranes: OH^- ion conductivity > 300 mS cm^{-1}[53]
Gating	Chloride transport (In response to various chemical and electrical stimuli)[54]	Photothermal MOF membrane (In response to light)[55]
Rectification	Cellular pH stabilization, ATP synthesis[56]	*In situ* synthesized HOF ion rectification membrane for osmotic energy harvesting[57]
Cooperative transport	The $KCNN_4$ channel (Ca^{2+}-activated K^+ channels)[58], cooperativity between the HCN channels[59]	Crown ether introduced in COF pores[60]

MOF: Metal-organic framework; COF: covalent organic framework; HCN: hyperpolarization-activated cyclic nucleotide-modulated.

BIONIC ION TRANSPORT IN 2D ORGANIC FRAMEWORK NANOFLUIDIC CHANNELS

Highly selective, rapid, and precisely controllable ion transport is critical for both biological and non-biological processes. Inspired by this, many important transport phenomena and gating mechanisms found in biological systems are now being reproduced using solid-state nanofluidic channels[49]. 2D organic framework featuring continuously interpenetrated pathways, a high density of pores with sub-nanometer size and designer physical and chemical surface properties could provide an ideal playground to realize controllable and rapid selective ion transport[50]. Table 1 compares the current status of ion transport functions in natural channels *vs.* 2D organic framework membranes[20,51-60]. While ion selectivity and ultrafast transport have been convincingly reproduced, their performance remains inferior to biological channels. Gating and rectification are only partially demonstrated with limited performance. Cooperative transport is still largely conceptual. These artificial systems have yet to match the sophistication of their biological counterparts, and further advances in both ion transport mechanisms and characterization techniques are still needed.

Ion transport mechanisms

Biological ion channels achieve transport rates approaching the diffusion limit while selectively excluding other species[33,61]. Such performance remains unattainable with current ion-selective materials. To achieve ultrafast permeation, 2D materials offer a distinct advantage: their atomic thickness provides the shortest possible transport path compared to traditional three-dimensional (3D) materials, drastically reducing transport resistance[12]. Meanwhile, several mechanisms have been proposed that could potentially govern this process, including size exclusion, surface charge effects, ion dehydration, *etc.*[62]. Replicating all these features in a single synthetic ion channel is unrealistic. Instead, one of the key advantages of artificial nanofluidic systems with respect to their biological counterparts is the structural simplicity enabling ease of fabrication and characterization. In this context, a more realistic developing strategy for man-made nanofluidic systems is to emulate some of the essential functions in biological systems using the simple and ideal nanofluidic pores or channels[63]. Ion transport through these man-made pores or channels is primarily governed by two key factors: channel dimensions and ion-wall interactions.

Surface charge

The channel surface plays a pivotal role in governing ion transport behavior. Specifically, the capacity to differentiate between cation and anion movement is regulated by electrostatic interactions mediated by surface charges. These electrostatic charges are driven by the dissociation of surface groups, isomorphic doping, or native crystallographic defects[64]. Once established, these charges interact with the surrounding electrolyte to form an electric double layer (EDL) near the channel walls, which selectively attracts

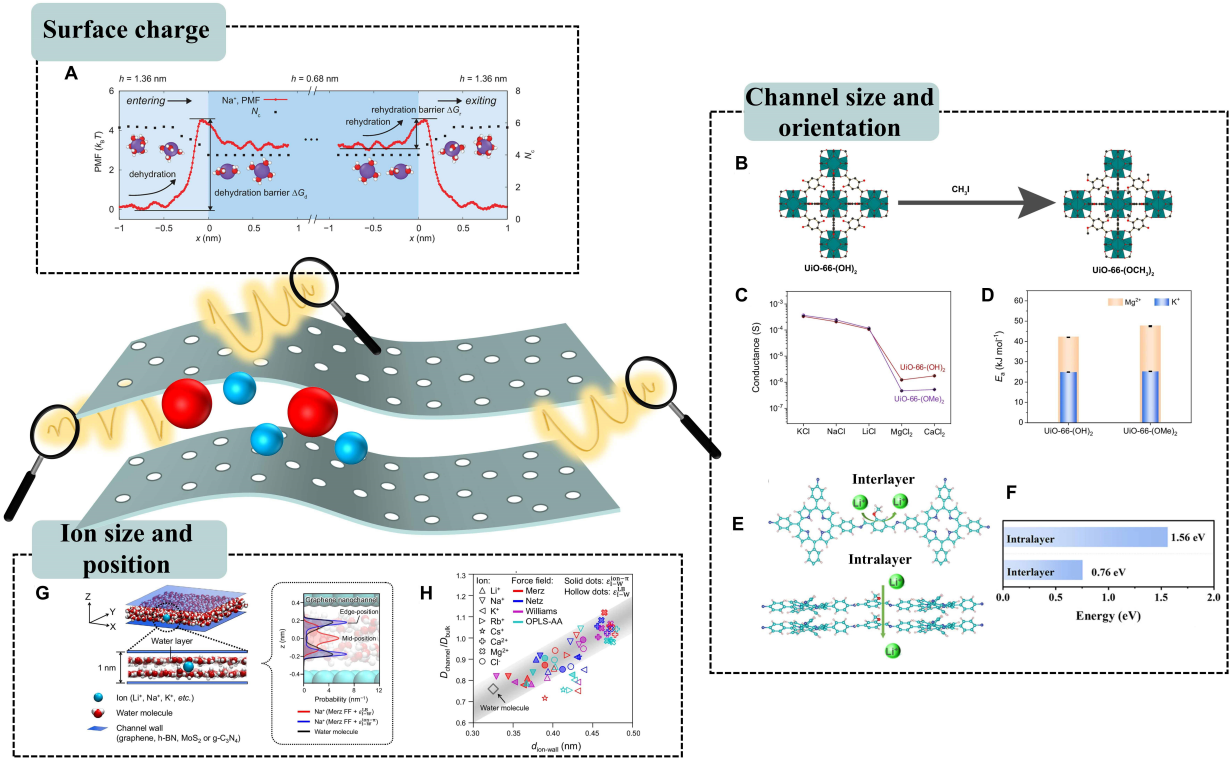

Figure 3. Ion transport mechanism in bionic nanofluidic channel. (A) Potential of mean force (PMF) and hydration number (N_c) for Na^+ entering/exiting a nanochannel. (A) Ref.[67] Copyright © 2020 American Chemical Society; (B) Structures of UiO-66-$(OH)_2$ and UiO-66-$(OCH_3)_2$; (C) Ionic conductance of UiO-66-$(OH)_2$ and UiO-66-$(OCH_3)_2$ membranes in 100 mM electrolyte solutions; (D) Activation energies governing K^+/Mg^{2+} transport across UiO-66-$(OH)_2$ and UiO-66-$(OMe)_2$ frameworks. (B-D) Ref.[81] Copyright © 2024, The Author(s); Schematic Li^+ migration along (E) parallel and vertical pathways with (F) corresponding energy barriers. (E and F) Ref.[85] Copyright © 2025 Wiley-VCH GmbH; (G) Simulation of hydrated ions in 2D nanofluidic channels; (H) The simulation of $D_{channel}/D_{bulk}$ with $d_{ion\text{-}wall}$ for various ions and force fields. (G and H) Ref.[93] Copyright © 2025, The Author(s). FF: Force fields; OPLS: optimized potentials for liquid simulations; AA: all-atom BN:boron nitride; $D_{channel}/D_{bulk}$: the ion self-diffusivity ratio of 2D nanochannels to bulk water; $d_{ion\text{-}wall}$: the distance of ion-wall.

counter-ions and repels co-ions. In nanofluidic systems, this ion selectivity is quantitatively characterized by the Debye screening length (λ_D), representing the effective thickness of the EDL[65]. When the channel width (d) is comparable to or smaller than λ_D ($d \leq \lambda_D$), EDL overlap occurs, leading to robust co-ion exclusion and preferential counter-ion transport. For ionic concentrations from 1 M to 1 μM, λ_D varies from approximately 1 to 100 nm. This range guides the design of charged nanochannels with dimensions matched to this scale to exploit EDL overlap for improved selectivity[66]. To allow quantitative assessment of the selective transport processes, Zhou *et al.* calculated the potential of mean force (PMF) to quantify ion entry energetics into a nanochannel with bare edges [Figure 3A][67]. The modularity of 2D organic frameworks enables the precise design of adaptive surface charges. For example, integrating dipolar benzothiadiazole units into COF nanochannels enables dynamic charge regulation via ion-dipole interactions[68]. Exposure to multivalent anions amplifies the negative surface charge, strengthening EDL overlap and enhancing cation perm-selectivity, whereas multivalent cations can reversibly invert the membrane polarity. This highlights how tailored pore chemistry actively modulates electrostatic interactions for tunable ion selectivity.

Notably, ion selectivity persists even when the d exceeds λ_D, extending to micrometer scales, indicating other mechanisms are involved. In such regimes, selectivity is no longer dictated by EDL overlap, but governed by the Dukhin number (*Du*), which evaluates the competition between ion-selective surface conductance ($G_{surface}$) and non-selective bulk conductance (G_{bulk})[69,70]:

$$Du = \frac{G_{\text{surface}}}{G_{\text{bulk}}} = \frac{|\sigma_s|}{ecr} = \frac{l_{Du}}{d}$$

where σ_s is the surface charge density, c denotes the bulk salt concentration, e is the elementary charge, and l_{Du} is the Dukhin length. Both the Du and l_{Du} describe the relative significance of surface and bulk contributions to conductance. When $d \leq l_{Du}$, surface conductance predominates, resulting in ion-selective transport. Impressively, experimental evidence from micropore systems further confirms that the Du can attain values as high as 10 in low-concentration electrolytes, validating the dominant surface conduction in micrometer-scale channels[71]. This indicates that surface conduction remains significant and non-negligible, and even surpasses bulk conduction, especially in dilute solutions. Crucially, this mechanism is expected to guide the design of 2D organic frameworks. The equation implies that maximizing σ_s sustains a high Du even in enlarged pores. By densely grafting charged functional groups onto 2D pore walls, researchers can exploit surface conduction to simultaneously achieve high ion flux (via wider channels) and precise selectivity, breaking the conventional permeability-selectivity trade-off[72].

Channel size and orientation

Ion selectivity in nanochannels can be achieved by utilizing the effective ionic size in solution. However, this strategy is inadequate for hydrated ions with comparable diameters[73]. Enhanced selectivity occurs when confinement dimensions match or fall below those of hydrated ions[74]. In 2D organic framework membranes, intrinsic pore structures and interlayer spacings define the effective channel length for ion transport. To enter these spaces, ions must overcome a free-energy barrier from partial dehydration or hydration shell reorganization at the channel entrance[75].

Shortening the channel length generally enhances ion permeability[76]. Membranes with single-atomic or molecular-layer thickness minimize mass transfer resistance, substantially increasing ion flux[77-79]. For example, Yang *et al.* designed monolayer COF membranes with well-defined pore structures. When integrated into salinity-gradient power generators using artificial seawater and river water, they delivered output power densities exceeding 200 W cm^{-2}[46]. In such ultrathin membranes, ion transport occurs perpendicular to the surface. In contrast to longer channels, where selectivity primarily arises from interactions between ions and the inner channel walls, the extremely short channel length precludes reliance on wall-mediated effects[64]. Instead, discrimination depends critically on a well-defined charged region surrounding the pore entrance. This suggests that an excessively high density of ion channels may decrease the selectivity of ultrathin membranes, as the interpore regions may become insufficient to sustain effective charge separation[80]. To investigate ion binding and dehydration in sub-nanometer channels of varying sizes, Mo *et al.* designed functionalized UiO-66-$(X)_2$ membranes with tunable channel dimensions (X = NH_2, SH, OH, and OCH_3 (OMe)[81]. Changing the functional group from OH to OMe left monovalent cation conductance largely unchanged, while significantly decreasing divalent cation conductance [Figure 3B-D]. This indicates that as the channel size decreases, monovalent cation transport is largely unaffected, whereas divalent cation transport is significantly hindered.

The orientation of nanochannels can also affect the channel length, which can be divided into horizontal and vertical orientations. Vertically oriented membranes, where ions permeate perpendicular to the laminated sheets, exhibit permeability up to three orders of magnitude higher than horizontally oriented ones. This ultrafast transport in vertically aligned channels is attributed to rapid ion entry, increased accessible surface area, and shortened diffusion pathways[82,83]. In 2D organic frameworks, nanochannel regulation is achieved primarily by designing molecular nodes and linkers within the porous nanosheets. Selecting building units

with dimensions matching the molecular size of target species enables precise control over channel size and ion selectivity[84]. Naren *et al.* revealed that lithium ions (Li^+) migrate within the COF cavities via two distinct pathways: an interlayer vertical channel and an intralayer parallel channel [Figure 3E][85]. The activation barrier for vertical migration is only 0.76 eV, less than half the 1.56 eV required for the parallel route, as the enlarged pore aperture relaxes steric constraints imposed by the 0.42 nm interlayer spacing. This enables Li^+ to hop directly through the pore interior rather than between adjacent sheets [Figure 3F][85].

Ion size and position

Membranes designed for cation separation, desalination, and proton conduction rely fundamentally on precise size exclusion. Under extreme confinement, the transport mechanism is dictated by the relative size between the channel diameter (D_C) and the ion's hydration diameter (D_H). In the regime where $D_C > D_H$, ions translocate freely with their primary solvation shells intact[86]. However, as D_C scales down ($D_C \leq D_H$), permeation forces ions to partially or fully shed their hydration shells. This dehydration process imposes a steep thermodynamic energy barrier, shifting transport into an activated translocation regime where permeation rates drop exponentially. In conventional 2D membranes, this steric exclusion implies that larger hydrated ions are either completely blocked or diverted through tortuous interlayer pathways, severely lowering permeability. In contrast, adequately sized species can directly traverse the intrinsic pores of 2D organic framework nanosheets, significantly enhancing permeability. For example, ideal desalination channels are engineered between the diameter of a water molecule (~ 0.28 nm) and typical hydrated ions (0.7-0.9 nm)[87]. Consistent with this, Corry *et al.* demonstrated that the precise cut-off size for NaCl rejection strictly falls within the 0.6-0.8 nm range[88]. Consequently, tailoring channel dimensions to exploit this hydration-dependent energy barrier, often in combination with specific pore functionalization to further modulate transport[89], remains the primary strategy for achieving precise ion sieving.

When ions pass through neutrally charged pores, their hydration shells size plays a decisive role in ion transport. Zhao *et al.* demonstrated that K^+ and Cl^- cannot permeate neutral pores with a 2 Å diameter, whereas both ions readily traverse 8 Å pores[90]. To allow ions to pass while retaining their hydration shells, pore diameters must exceed approximately 7 Å. In larger neutral pores, ionic transport is primarily limited by access resistance at the pore entrances and exits, well described by continuum electrokinetic theory[91,92]. Additionally, ion diffusion in 2D nanochannels is position-dependent. Liao *et al.* used molecular-dynamics simulations with multiple force fields to reveal a linear correlation between the diffusivity of ions with small first hydration shell (HS) radius (≤ rHS of K^+) and their distance from the channel wall ($d_{ion\text{-}wall}$)[93]. When $d_{ion\text{-}wall}$ is large, $D_{channel}/D_{bulk} > 1$. In contrast, for large rHS ions such as K^+, Rb^+ and Cs^+, $D_{channel}/D_{bulk}$ remains constant and is insensitive to $d_{ion\text{-}wall}$ [Figure 3G and H][93]. Quantitative analysis further elucidated the underlying physics by linking fundamental quantities, involving the water free-energy landscape around the ion, water residence time in the hydration shell, and the water-ion friction coefficient. As ion position can be tuned by external electric or magnetic fields, this mechanism offers a promising route to regulate ionic transport in 2D nanochannels for various applications[29,94].

Characterization techniques

The characterization of ion transport at the nanoscale has evolved significantly over the past two decades, driven by advances in nanofabrication and sensing technologies. Despite early progress in solid-state physics, systematic hydrodynamic and transport studies in confined fluidic environments remain challenging due to fabrication precision and signal-detection limitations[7]. Current methodologies can be broadly categorized into three classes: vesicle-based assays, conventional nanofluidic devices, and electrophysiological techniques [Figure 4].

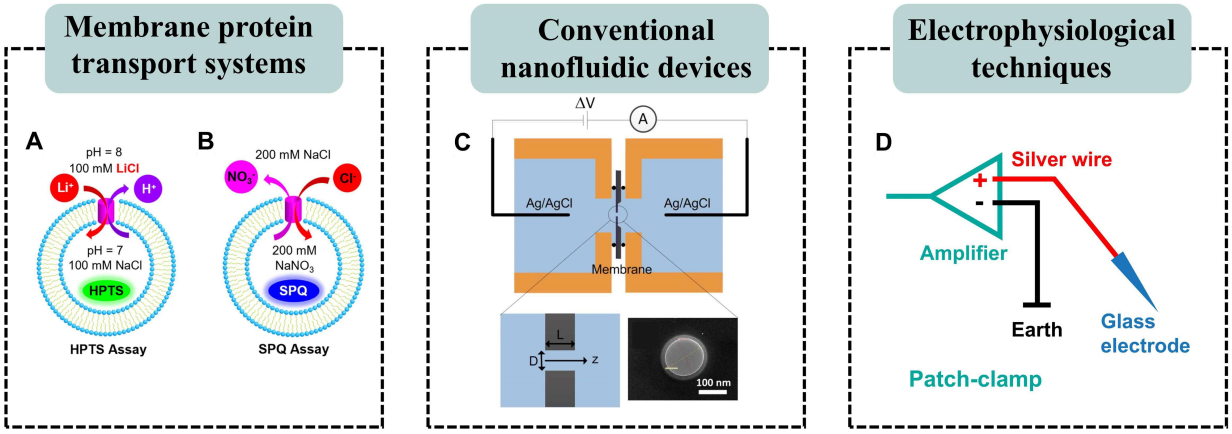

Figure 4. Classification of Characterization techniques for ion transport in nanofluidic channels. Schematic of (A) pH-sensitive HPTS assay, (B) SPQ assay. (A and B) Ref.[98] Copyright © 2023 Wiley-VCH GmbH; (C) Schematic of an ion-conductance flow cell. (C) Ref.[101] Copyright © 2012, American Chemical Society; (D) Schematic of basic components of the patch-clamp technique. HPTS: Pyranine; SPQ: 6-methoxy-N-(3-sulfopropyl)quinolinium.

Unilamellar vesicles, classified as small (SUVs, 20-100 nm), large (LUVs, 100-1,000 nm), or giant (GUVs, 1-200 μm), are widely used platforms for studying membrane protein-mediated ion transport[95,96]. SUVs and LUVs are favored for their ease of preparation, though their high curvature may artificially enhance transport rates. In contrast, GUVs mimic cellular dimensions and enable direct visualization via microscopy, thereby facilitating real-time imaging of channel insertion and membrane dynamics[97]. Fluorescent probes offer sensitive, real-time monitoring of ion flux. The pH-sensitive fluorescent dye HPTS (pyranine) detects H^+/OH^- movement across membranes, while SPQ [6-methoxy-N-(3-sulfopropyl)quinolinium] assesses anion permeability [Figure 4A and B][98]. Other commonly used dyes include Lucigenin (halide-sensitive), Safranin O (membrane potential indicator), and CF/calcein (integrity markers), which exhibit concentration-dependent fluorescence changes upon pore formation or leakage[95,99]. These assays typically establish ion gradients across lipid bilayers, and fluorescence changes following channel introduction allow kinetic analysis of transport activity[98,100]. Their simplicity, broad probe compatibility, and intuitive readouts make vesicle systems a versatile tool for evaluating diverse ion-conducting materials.

In a conventional nanofluidic ion transport experiment, devices separate two electrolyte-filled reservoirs, each with an electrode [Figure 4C][101]. Electrode-based detection is the most common technique due to its simplicity. For aqueous systems, silver-silver chloride electrodes are preferred for stability and low capacitive interference. For solvents like ionic liquids, platinum electrodes are suitable[102]. A major challenge encountered in single-pore studies is measuring tiny ion currents generated by driving forces[73], such as electric fields, pressure, or concentration gradients[103]. In these setups, the same electrodes apply the voltage and record the current. Drawing analogies to neuromorphic computing, novel setups for nanofluidic memristors mimic biological transport, enabling computational operations[104]. Beyond electrode-based methods, optical techniques also probe ionic transport[105]. Additionally, ion concentration can be quantified via inductively coupled plasma mass spectrometry using calibration curves correlating conductivity with concentration[106].

Electrophysiological techniques, including the patch-clamp and bilayer lipid membrane (BLM) methods, are of considerable significance when integrated with biological and nanofluidic electrochemical analyses. The patch-clamp technique employs a fine glass pipette applied to the cell membrane to measure ionic currents passing through embedded ion channels [Figure 4D][107,108]. It offers high spatial and temporal resolution for real-time monitoring of ion transport. This enables precise detection of current fluctuations during channel

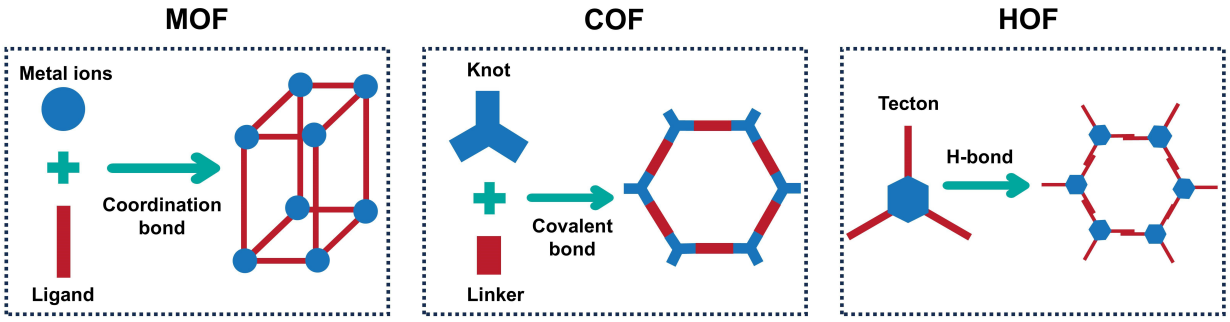

Figure 5. Typical structural and synthesis comparison of MOF, COF, and HOF. MOF: Metal-organic framework; COF: covalent organic framework; HOF: hydrogen-bonded organic framework.

activation and deactivation, facilitating molecular-scale analysis of current thresholds, gating probabilities, and other single-channel characteristics. Despite its efficacy in living cells, this method is limited by technical complexity and high costs. In contrast, the BLM approach examines ion transport through individual channels or nanopores in synthetic planar lipid bilayers. Although signals can arise from non-channel molecules, ion currents recorded in BLM experiments are considered the most direct evidence of functional channel formation[95]. In a standard setup, cis and trans chambers are connected to the amplifier headstage via KCl-agar bridges and Ag/AgCl electrodes. Channel molecules are introduced into the cis side, and an applied potential drives ion flux across the membrane. The resulting current response is recorded in real time, with a representative trace. The channel exhibits two distinct states, which are closed at negative voltages and open at positive voltages. At intermediate voltages, it interconverts repeatedly between these two states[109].

Resolving confined ion transport requires a careful consideration of technique-specific boundaries and limitations. Vesicle-based assays excel at high-throughput ensemble screening within lipid environments, but they lack single-channel resolution and high membrane curvature can artificially alter transport kinetics. Conventional nanofluidic devices accommodate diverse driving forces like pressure and concentration gradients, yet they struggle to detect tiny currents and fail to resolve localized spatial variations within heterogeneous structures. Electrophysiological techniques deliver unmatched spatial and temporal resolution for single-channel gating dynamics, but suffer from high technical complexity and bilayer fragility.

ENGINEERING 2D ORGANIC FRAMEWORK NANOFLUIDIC MEMBRANES

The preparation of 2D organic framework membranes typically involves two steps. The first step is the synthesis of single-layer frameworks with tailored structures, which can be engineered to incorporate pores of diverse sizes and shapes, thereby significantly enhancing topological diversity. In the second step, these 2D materials are assembled into macroscopic membranes using various fabrication techniques[110].

Typical structures of 2D organic framework nanofluidic membranes

2D organic materials, including 2D MOFs, COFs, and HOFs, are generally synthesized via bottom-up approaches. This enables precise structural control so that ion transport through the high-density pores in the basal planes can be measured and the underlying structure-property relationship can be elucidated. Figure 5 compares the typical structures and synthetic strategies of MOF, COF, and HOF. The capacity of these organic frameworks to emulate natural ion channels is inherently rooted in reticular design principles. By linking specific molecular building blocks through defined interactions, this methodology allows researchers to rationally build frameworks with predetermined topologies. This predictable assembly generates robust and customizable crystalline frameworks, making it possible to precisely design materials that mimic biological ion channels[111,112].

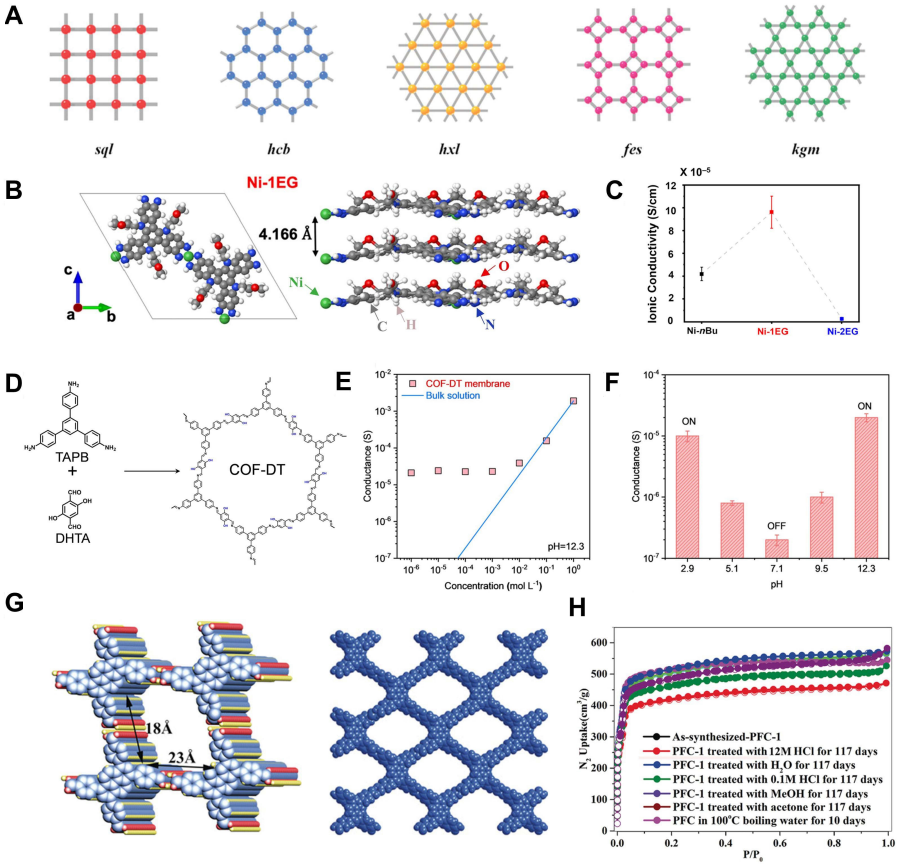

Figure 6. Typical 2D MOFs, 2D COFs and 2D HOFs structure-property correlations. (A) Schematic of some typical topologies of 2D MOFs networks: *sql*, *hcb*, *hxl*, *fes*, and *kgm*. (A) Ref.[114] Copyright © 2020 WILEY-VCH Verlag GmbH & Co. KGaA, Weinheim; (B) Illustration of Ni-MOF geometry. (C) Ionic conductivity of Ni-MOFs. (B and C) Ref.[118] Copyright © 2025, American Chemical Society; (D) Solvothermal synthetic reaction of the COF-DT membrane from TAPB and DHTA. (E) Ion conductance as a function of KCl concentration at pH = 12.3. (F) pH-responsive ion-gating of COF-DT membranes. (D-F) Ref.[122] Copyright © 2021 Wiley-VCH GmbH; (G) PFC-1 crystal structure of channel and porous framework. (H) N_2 adsorption isotherms for as-synthesized and solution-treated PFC. (G and H) Ref.[123] Copyright © 2018 Wiley-VCH Verlag GmbH & Co. KGaA, Weinheim. *sql*: square; *hcb*: honeycomb; *hxl*: hexagonal; *fes*: four-eight square; *kgm*: kagomé; EG: ethylene glycol; TAPB: 1, 3, 5-tris (4-aminophenyl)-benzene; DHTA: (2, 5-dihydroxy-1, 4-benzenedicarboxaldehyde; COF-DT: a covalent organic framework synthesized from DHTA and TAPB; PFC: porous materials from the Fujian Institute of Research on the Structure of Matter, Chinese Academy of Sciences; MOF: metal-organic framework; COF: covalent organic framework; HOF: hydrogen-bonded organic framework.

2D MOFs

MOFs are porous crystalline materials composed of metal nodes coordinated by organic linkers. Unlike 3D counterparts, 2D MOFs feature layered structures with in-plane connectivity[113]. They offer large surface areas, tunable pore structures, and well-defined topological networks, including honeycomb (*hcb*), four-eight square (*fes*), square (*sql*), kagomé (*kgm*), and hexagonal (*hxl*) [Figure 6A][114]. Rational design often relies on transition metals with predictable coordination geometries, such as Cu^{2+} and Zn^{2+}, combined with rigid organic ligands. Porphyrin derivatives are effective building blocks for 2D networks due to their structural rigidity, high connectivity, and planar conjugated macrocyclic frameworks[115,116]. Additionally, combining trigonal ligands with square-planar metal centers enables hexagonal layered MOFs[117]. These tailored 2D MOFs exhibit unique functionalities, such as mixed ionic-electronic conductors. For instance, Roh *et al.* showed that grafting ionophilic ethylene glycol (EG) groups onto a conductive MOF (cMOF) backbone enables high ionic conductivity (1.1×10^{-4} S/cm) [Figure 6B and C][118]. This exemplifies how side-chain engineering can decouple and control ionic and electronic transport[118].

2D COFs

2D COFs are an emerging class of porous crystalline materials featuring layered architectures formed via covalent bonding between π-conjugated building blocks[119]. Unlike graphene oxide (GO), graphene, molybdenum disulfide (MoS_2), or boron nitride (BN), 2D COFs possess intrinsic nanopores serving as nanochannels for efficient molecular and ion transport[120]. Realizing functional 2D COFs for nanofluidics requires precise pore engineering to establish structure-property relationships. This typically involves two strategies: (1) tailoring the pore chemistry by selecting linkages and framework units; (2) controlling the pore size, geometry, and arrangement by assembling building units with defined shapes. For the first strategy, choosing dynamic covalent bonds, such as B-O or C=N linkages, critically affects the stability and crystallinity[121]. Additionally, incorporating substituent groups, metal clusters, or heteroatoms via predesign or post-synthetic modification enables customization. Regarding the second strategy, common geometries include trigonal, tetragonal, hexagonal, and rhombic ones, which are formed by combinations such as C_3 + C_2, C_4 + C_2, C_2 + C_2, or 'T'+'C_2[119]. For instance, a COF-DT membrane with pH-responsive gating behavior was fabricated by designing a C_3 + C_2 topology functionalized with hydroxyl groups [Figure 6D-F][122].

2D HOFs

2D HOFs are porous materials assembled via hydrogen bonding and other noncovalent interactions, including π-π stacking and van der Waals forces[123,124]. While sharing some common structural features with MOFs and COFs, 2D HOFs are constructed via weak, reversible hydrogen bonds, endowing them with distinctive properties like self-healing, mild synthesis conditions, and solution processability. The synthesis of HOFs typically proceeds under ambient conditions via solvent evaporation-induced recrystallization, facilitated by high precursor solubility in organic solvents. Moreover, hydrogen bond flexibility and reversibility contribute to the regeneration of HOFs[125]. In 2D HOFs, stability is often enhanced by incorporating building blocks with extended π-conjugated systems. These frameworks benefit from synergistic in-plane hydrogen bonding and out-of-plane π-π stacking. Typically, organic units assemble via hydrogen bonds into 2D layers, which then stack via π-π interactions to form 3D architectures with 1D open channels aligned along the stacking direction. Among reported topologies, the 2D *sql* is most commonly used for stable 2D HOFs[126,127]. Liu *et al.* synthesized PFC-1 from 1,3,6,8-tetrakis(p-benzoic acid)pyrene (H_4TBAPy), a building block with a π-conjugated pyrene core and four benzoic acid arms. Each H_4TBAPy unit connects to four neighbors via cyclic carboxylic acid dimers, forming 2D *sql* hydrogen-bonded sheets[123]. These sheets stack in an AA mode along the [100] direction via π-π interactions (interlayer spacing ≈ 3.34 Å), generating 1D square channels (~ 18 × 23 Å) within a 3D open framework [Figure 6G]. The material exhibits a BET surface area of 2,122 $m^2 g^{-1}$ and retains crystallinity after immersion in concentrated HCl for 117 days [Figure 6H][123].

In summary, while MOFs, COFs, and HOFs share substantial surface areas, tunable pore structures, and an excellent capacity for surface functionalization, their distinct intrinsic bonding interactions fundamentally drive differences in structural stabilities and ion transport mechanisms[128,129]. Assembled via coordination bonds, MOF membranes provide exceptional chemical diversity. Their specific transport pathways and selectivity are heavily governed by controllable host-guest interactions at open metal centers and versatile organic linkers[130]. COF membranes are bridged by robust covalent bonds, granting them high chemical stability essential for practical precision separations. 2D COFs typically feature rigid, vertically aligned one-dimensional channels that minimize transport resistance, enabling ultrafast ion flow and precise steric sieving to overcome the permeability-selectivity trade-off[131]. Meanwhile, HOFs are assembled through non-covalent interactions, resulting in highly biocompatible and dynamic pore structures that naturally govern their transport behaviors. Specifically, continuous hydrogen-bonded networks formed by Brønsted acid-base pairs serve as intrinsic conduits for efficient proton conduction, while specific functional sites like unprotonated carboxylic groups endow the membranes with remarkable ion selectivity[132,133].

Table 2. Systematic comparison of 2D MOF, COF and HOF membranes[137-140]

Materials	Advantages	Disadvantages	Optimal applicable scenarios
2D MOF[137-140]	Precise pore size control	Low scalability	Osmotic power generation, proton conductor
2D COF[137-140]	High stability	Low structural flexibility	Energy storage, water desalination
2D HOF[137]	Facile synthesis	Low stability	Biomedical

MOF: Metal-organic framework; COF: covalent organic framework; HOF: hydrogen-bonded organic framework.

Despite the inherent advantages described above, specific dynamic linkages within COFs and the fundamentally weaker non-covalent networks of HOFs can still face degradation under extreme, long-term operational conditions. To address these bottlenecks, the chemical durability of imine-linked COFs prone to hydrolytic cleavage can be secured through stepwise post-synthetic functionalization into amide and pyridine N-oxide groups, which successfully preserves structural crystallinity even after 24-h exposure to 10 M strong acids and bases[134]. Alternatively, a linkage-encoding strategy embeds fully conjugated enaminone bonds into the backbone, allowing the membrane to maintain its macroscopic morphology, long-range order completely, and vertically aligned nanochannels after 24-hour immersion in 12 M sulfuric acid at 110 °C or 5 M potassium hydroxide, drastically outperforming conventional imine or incompletely tautomerized ketoenamine networks[135]. For HOFs, permanent porosity can be stabilized against activation collapse by incorporating cooperative hydrogen bonding and π-π interactions to lock the organic building units[133]. For instance, incorporating metal ions into porphyrin frameworks yields robust architectures that maintain structural integrity under 270 °C thermal stress and remain crystalline in concentrated hydrochloric acid for 24 h[136]. These organic framework membranes exhibit distinct intrinsic advantages and limitations, which directly determine their optimal application scenarios [Table 2][137-140].

Representative membrane assembly strategies

Practical application of crystalline porous materials requires integrating them into membranes via tailored fabrication methods that preserve structural order and functionality. For instance, COFs feature highly ordered and densely aligned pore structures, which require tailored membrane fabrication techniques to fully exploit their capabilities. Meanwhile, developing effective methods to minimize defects in polycrystalline membranes is crucial for achieving high separation performance. Furthermore, improving the adhesion or interfacial bonding between the selective layer and the substrate is critical to ensure mechanical stability. This section reviews strategies for fabricating high-performance crystalline porous membranes.

Solution processing

Solution processing is ideal for fabricating membranes from organic framework materials with good solvent dispersibility and stability[141]. Among solution-based methods, vacuum filtration is particularly efficient and scalable for producing 2D organic framework membranes. For instance, Jian *et al.* exfoliated 2D monolayer nanosheets of an aluminum tetra-(4-carboxyphenyl) porphyrin framework (Al-MOF)[142]. Then they assembled an ultrathin, continuous Al-MOF membrane by vacuum filtering a dilute nanosheet suspension onto an anodic aluminum oxide (AAO) support[142]. In polar solvents, HOFs evolve into small particles while retaining intrinsic crystalline order due to surface polar groups (e.g., -NH_2, -COOH) that do not participate in the internal hydrogen-bonding network. These exposed groups interact effectively with polar solvents like N-methylpyrrolidone (NMP), Dimethyl sulfoxide (DMSO), and N, N-dimethylformamide (DMF), enabling homogeneous dispersion and high-quality membrane fabrication[133,143]. However, solution processing via vacuum filtration requires large nanosheets to exceed substrate pore sizes for effective retention, which induces rapid, forced deposition and misaligned assembly. Although individual flakes preserve their intrinsic crystallinity, the macroscale structure suffers from disordered amorphous voids between layers[144]. To address this limitation, Duan *et al.* used hydrophilic polymers, polyvinyl alcohol (PVA) and polyethylene

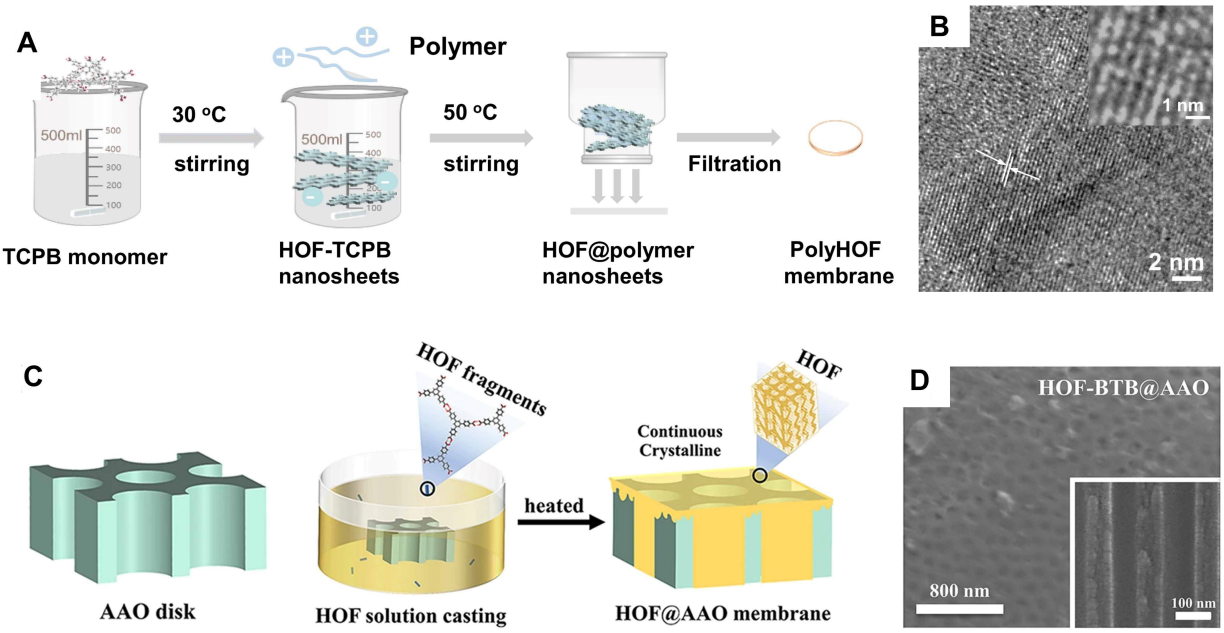

Figure 7. (A) Synthesis of HOF-TCPB nanosheets and PolyHOF membrane. (B) TEM images of HOF-TCPB nanosheets. (A and B) Ref.[145] © The Author(s) 2025. Published by Tsinghua University Press; (C) Preparation of HOF@AAO membrane through a solution-casting approach. (D) Top-view SEM of HOF-BTB@AAO membrane. (C and D) Ref.[143] Copyright © 2024, The Author(s). HOF: Hydrogen-bonded organic framework; BTB: 1,3,5-Tris(4-carboxyphenyl)benzene; TCPB: 1,2,4,5-tetrakis(4-carboxyphenyl)benzene; AAO: anodic aluminum oxide; SEM: scanning electron microscope.

glycol (PEG), to form multiple-site hydrogen bonding with HOF monomers, namely, 1,2,4,5-tetrakis(4-carboxyphenyl)benzene (TCPB)[145]. The flexible polymer chains promoted tight stacking during vacuum filtration, enhancing the crystallinity and stability of the resulting lamellar membranes [Figure 7A and B][145].

In addition to vacuum filtration, Sun *et al.* pioneered solution-processing HOF membranes by optimizing precipitation conditions[146]. They constructed a flexible and stable HOF (UPC-HOF-6) using a triangular building block, 4′,4″,4‴-nitrilotris[([1,1′-biphenyl]-4-diaminotriazine)] (NBP-DAT). The UPC-HOF-6 was dissolved in DMSO at various concentrations and coated onto AAO substrates[146]. To elucidate the solution processability of well-defined HOFs, Yin *et al.* investigated the aggregation of a porous and crystalline HOF material (HOF-BTB) dispersed in solvent [Figure 7C][143]. Cryo-electron microscopy showed that the nanoscale fragments (10-150 nm) retained the bulk crystal structure. On the basis of these insights, a highly crystalline and continuous HOF membrane was successfully fabricated on macroporous AAO disks [Figure 7D], demonstrating the broad applicability of the described approach for different HOFs, solvents, and substrates[143]. Despite its versatility, solution processing requires meticulous optimization to minimize residual solvent-induced defects that could cause pore blockage and compromise membrane performance.

Interfacial polymerization

Interfacial polymerization (IP) is a facile, scalable method for fabricating large-area thin films for 2D COF membranes. This technique exploits reactions at liquid-liquid interfaces to generate continuous membranes with controlled thickness and morphology. Dey *et al.* pioneered a bottom-up interfacial crystallization strategy for COF membrane fabrication, wherein an aldehyde linker was dissolved in dichloromethane (organic phase) and then reacted with an amine monomer in water (aqueous phase) [Figure 8A][147]. Slow diffusion at the interface yielded crystalline Tp-Bpy membranes, enabling simultaneous control over crystallization kinetics and morphology [Figure 8B][147]. Similarly, Zhu *et al.* utilized IP to coordinate metal ions within a COF film, reorienting random nanochannels into axially aligned arrays that boosted ion

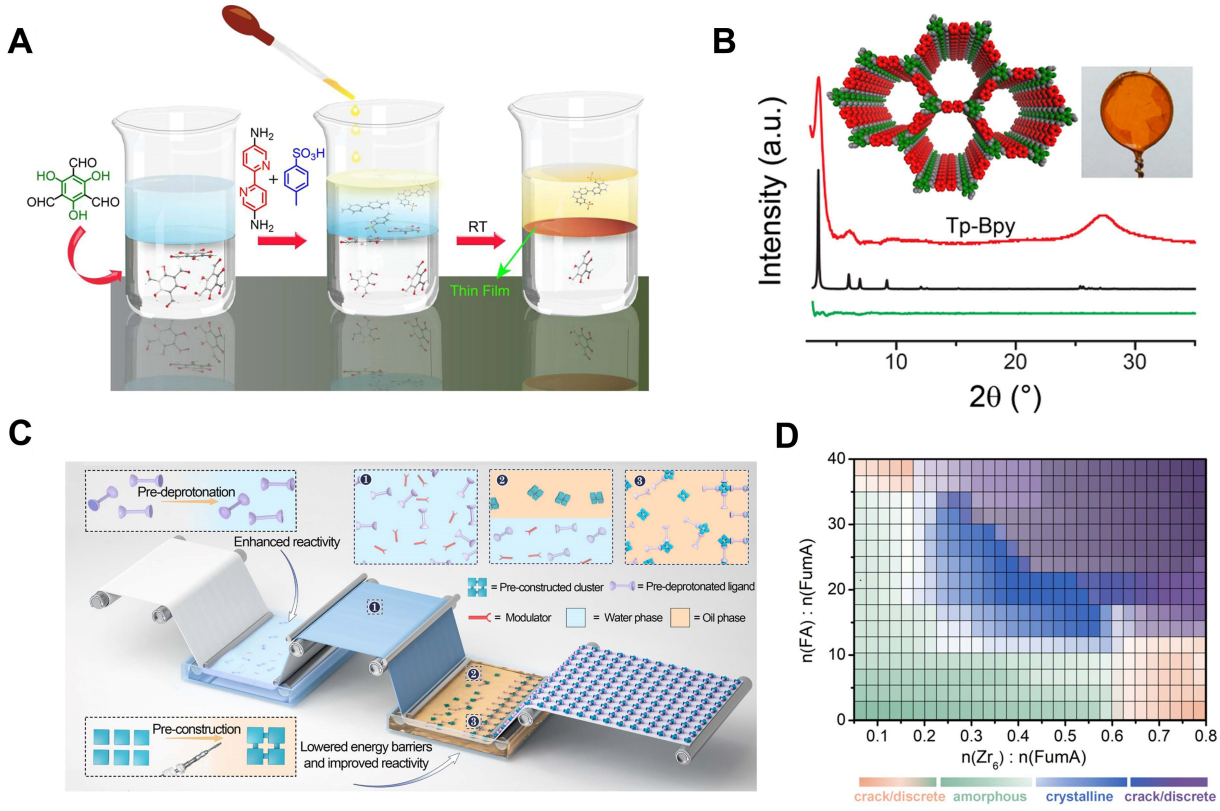

Figure 8. Construction of 2D organic framework membranes through IP. (A) Interfacial crystallization scheme for Tp-Bpy COF film formation; (B) X-ray diffraction patterns of Tp-Bpy COF thin films with inset image of freestanding thin films. (A and B) Ref.[147] Copyright © 2020 The Authors; (C and D) Roll-to-roll PMIP fabrication and continuity/crystallinity heat map of Zr-fum-MOF membranes. (C and D) Ref.[152] Copyright © 2020 The Authors. RT: Room temperature; Tp: 1,3,5-triformylphloroglucinol; Bpy: 2,2′-bipyridine-5,5′-diamine; IP: interfacial polymerization; PMIP: preformed metal cluster interfacial polymerization; COF: covalent organic framework.

selectivity and permeability for osmotic energy and nanofluidic applications[148]. Besides separating the two monomers into distinct phases, Matsumoto *et al.* co-dissolved both amine and aldehyde monomers in a single organic phase with a Lewis acid catalyst $Sc(OTf)_3$ in the aqueous phase[149]. IP at the phase boundary yielded continuous 2D imine-linked COF films with lateral dimensions limited only by the vessel size. By tuning monomer concentration, film thickness was controlled from 10 μm down to 2.5 nm[149].

The IP method has been extensively employed in the construction of COF membranes. In MOF synthesis, it has mainly focused on low-valent metal cations that are readily activated at low temperatures, such as Zeolitic Imidazolate Framework-8 (ZIF-8)[150]. Synthesizing high-valent cluster-based MOF membranes (e.g., Zr, Cr, Fe) remains challenging due to high energy barriers and complex formation mechanisms[151]. To overcome this difficulty, Sun *et al.* employed pre-synthesized metal clusters (e.g., Zr-clusters), circumventing energy-intensive *in situ* formation. Combined with roll-to-roll processing on flexible polymer supports, the preformed metal cluster interfacial polymerization (PMIP) enables continuous fabrication of Zr-fum-MOF membranes at ambient temperature [Figure 8C and D]. IP is advantageous for producing large-area, flexible membranes compatible with diverse polymeric substrates[152]. However, the conventional interfacial polymerization method often yields membranes with a low crystalline fraction, typically ranging from 16.47% to 73.90%, which constrains the precision of molecular sieving[153]. Furthermore, scaling up conventional interfacial polymerization compromises macroscale uniformity. To resolve this, Zhang *et al.* developed a reverse-phase microemulsion strategy using an ionic liquid network to prearrange monomers, enabling concurrent polymerization and crystallization within seconds. Combined with a scraping-assisted process, this method yielded highly crystalline COF membranes at a meter scale of 0.4 by 1.0 meters[154].

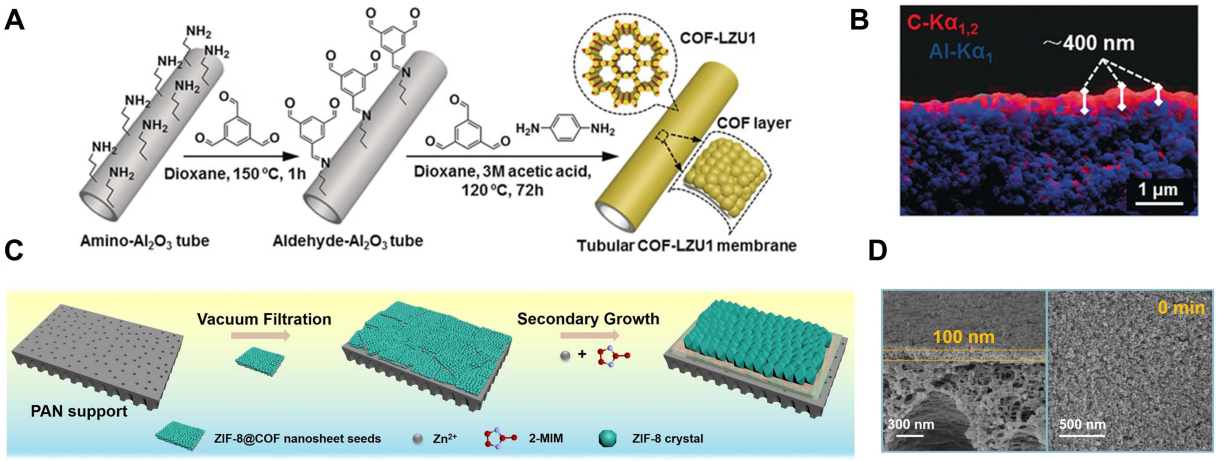

Figure 9. Construction of 2D organic framework membranes through *in situ* growth. (A and B) Synthesis and EDXS mapping of tubular COF-LZU1 membrane. (A and B) Ref.[156] Copyright © 2018 Wiley-VCH Verlag GmbH & Co. KGaA, Weinheim; (C and D) Schematic and SEM images of ZIF-8@TpPa-SO_3H via secondary growth. (C and D) Ref.[160] Copyright © 2023 Wiley-VCH GmbH. COF-LZU1: A covalent organic framework (LZU: Lanzhou University); PAN: polyacrylonitrile; ZIF: zeolitic imidazolate framework; EDXS: energy-dispersive X-ray spectroscopy; SEM: scanning electron microscope.

In situ growth

In situ growth, including solvothermal and seed-assisted secondary growth, is widely used for synthesizing organic framework membranes, particularly those based on MOFs and COFs[19]. A significant advancement in solvothermal synthesis began in 2009 with the work of Liu *et al.*, who successfully fabricated the first MOF-5 membrane via *in situ* solvothermal growth on a porous alumina substrate[155]. The resulting polycrystalline membrane exhibited continuous morphology, demonstrating the feasibility of directly growing MOF layers on supports. This approach was then extended to various MOF systems and adapted for 2D COFs. For instance, Caro *et al.* functionalized ceramic tubes with 3-aminopropyltriethoxysilane (APTES), followed by reacting with 1,3,5-triformylbenzene (TFB) to create a surface-anchored ligand layer [Figure 9A]. Vertical placement of these tubes in an autoclave with p-phenylenediamine (PDA) yielded well-intergrown, 400 nm thick tubular COF-LZU1 membranes [Figure 9B][156]. While *in situ* solvothermal synthesis produces highly crystalline and coherent membranes, anisotropic growth kinetics often lead to challenges in controlling crystal orientation[19,157]. This misalignment generates defect pores exceeding 1 nm, which surpass the size of the intrinsic fundamental unit pores typically below 1 nm[158].

Despite considerable advancements in *in situ* solvothermal membrane fabrication, further reducing the membrane thickness remains challenging due to scarce nucleation sites[159]. To address this limitation, seed-assisted secondary growth techniques have been developed to enhance flux. In 2023, Pu *et al.* introduced negatively charged COF nanosheets as porous substrates that are capable of selectively adsorbing Zn^{2+} ions[160], and then deprotonated 2-methylimidazole (2-MIM) ligands coordinated with surface-enriched Zn^{2+}, initiating heterogeneous nucleation [Figure 9C]. This strategy produced ZIF-8@COF nanosheet seeds, yielding ZIF-8 membranes as thin as 100 nm [Figure 9D]. While seed-assisted secondary growth enables ultrathin, high-permeance membranes, it requires precise control over seed-layer uniformity and orientation, increasing procedural complexity. Furthermore, secondary growth parameters (for example, temperature, duration, precursor concentration) critically influence the membrane quality, which requires meticulous optimization[157,161].

Liquid-air interface self-assembly

Liquid-air interface synthesis is an effective strategy for fabricating membranes by guiding molecular assembly at the interface[162]. This method typically involves the self-assembly of amphiphilic monomers at

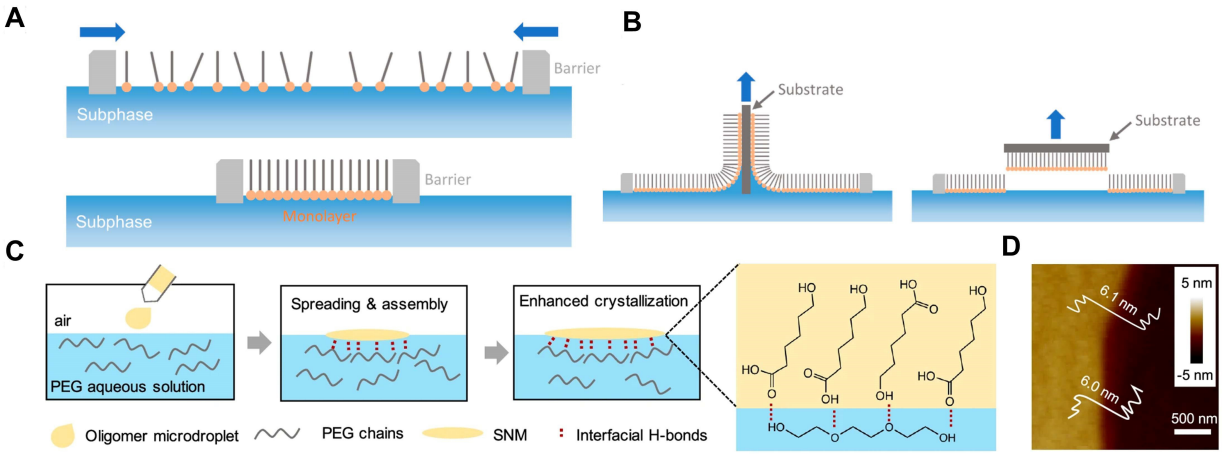

Figure 10. Construction of 2D organic framework membranes through liquid-air interface self-assembly. Langmuir-Blodgett method for (A) dense monolayer formation via barrier compression and (B) subsequent substrate transfer. (A and B) Ref.[169] Copyright © 2022, American Chemical Society; (C) Schematic of PCL nanofilm preparation at the air/PEG aqueous solution interface; (D) AFM of SNM-2. (C and D) Reproduced under the CC-BY-NC license from Ref.[173] Copyright © 2025, The Author(s). PEG: Polyethylene glycol; SNM: supramolecular nanocrystal membrane; PCL: polycaprolactone; AFM: Atomic force microscopy.

the interface, followed by *in situ* polymerization or cross-linking to form large-area, ordered ultrathin membranes with well-defined nanochannels[163]. To promote polymer chain alignment and crystallization (e.g., within microscale droplets at the interface), the following factors are critical: a positive spreading coefficient for rapid, large-area film expansion, and abundant interfacial binding sites to enrich polymer chains via interfacial interactions. Satisfying these conditions enables tightly packed, highly oriented polymer arrangements within short time scales, thereby enhancing crystallinity at the interface[164,165]. Zhang *et al.* fabricated highly crystalline COF films via a gas-liquid interface method. The films exhibit a highly ordered tetragonal lattice with single crystal domains exceeding 10^4 nm^2[166].

The Langmuir-Blodgett (LB) technique utilizes amphiphilic molecules with hydrophilic heads and hydrophobic tails. These molecules spontaneously assemble into monolayer or multilayer films at the water-air interface, where lateral compression induces ordered molecular packing. The resulting films are then transferred onto solid substrates to form uniform layers[167-169] [Figure 10A and B]. Leveraging interfacial confinement and directional interactions, the LB technique precisely regulates molecular conformation and orientation. For example, Mao *et al.* fabricated a cationic AB-stacked COF bilayer using molecular design and the LB method[170]. The structure features highly ordered sub-2 nm pores, an atomic thickness of 1.3 nm, exceptional pore utilization, and a high surface charge density of 4.4 mC m^{-2}[170]. Similarly, Makiura *et al.* demonstrated room-temperature bottom-up fabrication of NAFS-1, a preferentially oriented ultrathin porphyrinic MOF nanofilm with long-range crystalline order in both in-plane and out-of-plane directions[171]. Integrating layer-by-layer and LB methods with metal-coordinated pyridine linkers drives interdigitated growth, offering a versatile solution-based route for well-controlled MOF nanofilms in sensors, catalysts and fuel-cell electrodes[171]. Despite its molecular-level precision, the LB technique is constrained by limited monomer selection, low collapse pressures, and low transfer yields[169,172].

Similar to the LB method, Lu *et al.* developed a supramolecular nanocrystal membrane (SNM) using interfacial hydrogen bonding in nanoconfined spaces[173]. Mediated by polyethylene glycol (PEG), the interaction guided the ordered arrangement of polycaprolactone (PCL) chains into a continuous nanofilm [Figure 10C]. The resulting SNM features large crystal domains (100-150 nm) and a thickness of 6 nm [Figure 10D]. These domains contain abundant, ordered sub-nanometer channels that form continuous water pathways and align water molecules, thereby increasing the energy barrier for sodium ion transport

Table 3. Comparison of different fabrication strategies for organic framework membranes[141,145,150,157,159,168,172]

Fabrication strategy	Applicable material types	Advantages	Disadvantages	Representative performance indicators
Solution processing[141,145]	Nanosheets suspensions	High scalability, low cost, simple operation	Restacking voids	High solvent permeability
Interfacial polymerization[150]	Linkers or monomers	Ultra-thin, rapid reaction kinetics	Low crystallinity	High desalination rejection
In situ growth[157,159]	Organic linkers coupled with surface seeds	Highly crystalline and coherent	Slow kinetics	High separation selectivity
Liquid air interface self-assembly[168,172]	Amphiphilic monomers	Precise atomic thickness, ordered orientation	Fragile substrate transfer	Ultrahigh ion flux

while enhancing water flux[173]. A comprehensive comparison of these fabrication strategies is summarized in Table 3[141,145,150,157,159,168,172].

APPLICATIONS OF 2D ORGANIC FRAMEWORK MEMBRANES IN NANOFLUIDICS

2D nanofluidic membranes offer a unique platform for modulating ion transport through well-defined nanochannels[174,175]. Unlike inorganic 2D materials (e.g., GO, vermiculite), 2D organic framework nanosheets possess intrinsic nano- or subnanometer-scale pores across their basal planes. Consequently, laminar membranes assembled from stacked 2D organic frameworks achieve high selectivity thanks to the surface chemistry and strong confinement in the interlayer channels and high permeability due to intrinsic nanopores serving as additional transport pathways[176]. They hold great promise for applications such as desalination, energy conversion and storage, proton conductors, and artificial synapses.

Desalination

Seawater desalination offers a viable solution to the global freshwater crisis[177]. It is primarily implemented through thermal distillation but recently, due to energy concerns, membrane-based separation is believed to be an alternative route[178]. Because of the high surface area, tunable pore shapes and sizes, diverse surface chemistry, and chemical stability, 2D organic framework membranes are promising candidates for next-generation desalination[179]. Zhao *et al.* synthesized a 2D COF membrane with a hydrophilicity gradient for molecular distillation, demonstrating exceptional performance in dealing with highly saline, contaminated water[180]. The COFDT-E18@cPVDF membrane achieved > 99.99% NaCl rejection and a water flux of 370 $L \cdot m^{-2} \cdot h^{-1}$ at 75 °C with 3.5 wt% NaCl under 16 kPa. Also, a three-unit module (27 cm^2 total area) equipped with such membranes purified 4 L of Bohai seawater over 10 h and removed 99.99% of salts[180].

The hourglass-shaped nanochannel, featuring a narrow spout flanked by wider entrances, is a promising design for desalination[181]. Wei *et al.* constructed a 2D COF membrane by anchoring amino-cyclodextrin nanoparticles (CDNs) at the pore mouths [Figure 11A][182]. The resulting hetero-channel comprised a hydrophilic tapered entrance (~ 1.6 nm), a hydrophobic constriction (~ 0.5 nm) defined by the CDN cavity, and intrinsic COF pores (~ 1.4 nm). The hydrophilic entrance promoted water absorption, while the hydrophobic constriction and intrinsic pores synergistically accelerated water flow. Additionally, CDN amino groups imparted pH-responsive behavior, whereby the pore sizes and charges could be effectively adjusted. The COF-CDN membrane achieved a water flux of 98 L m^{-2} h^{-1}, with 94% Na_2SO_4 and 92% NaCl rejection. It remained stable for over 7 days across varying pH conditions, highlighting its potential for efficient desalination [Figure 11B].

Osmotic energy conversion

Osmotic energy, generated from salinity gradients between freshwater and seawater, is a promising renewable source[183]. However, its practical application is hindered by the low power output of traditional ion-exchange membranes, which suffer from poor ionic selectivity and high internal resistance. The typical

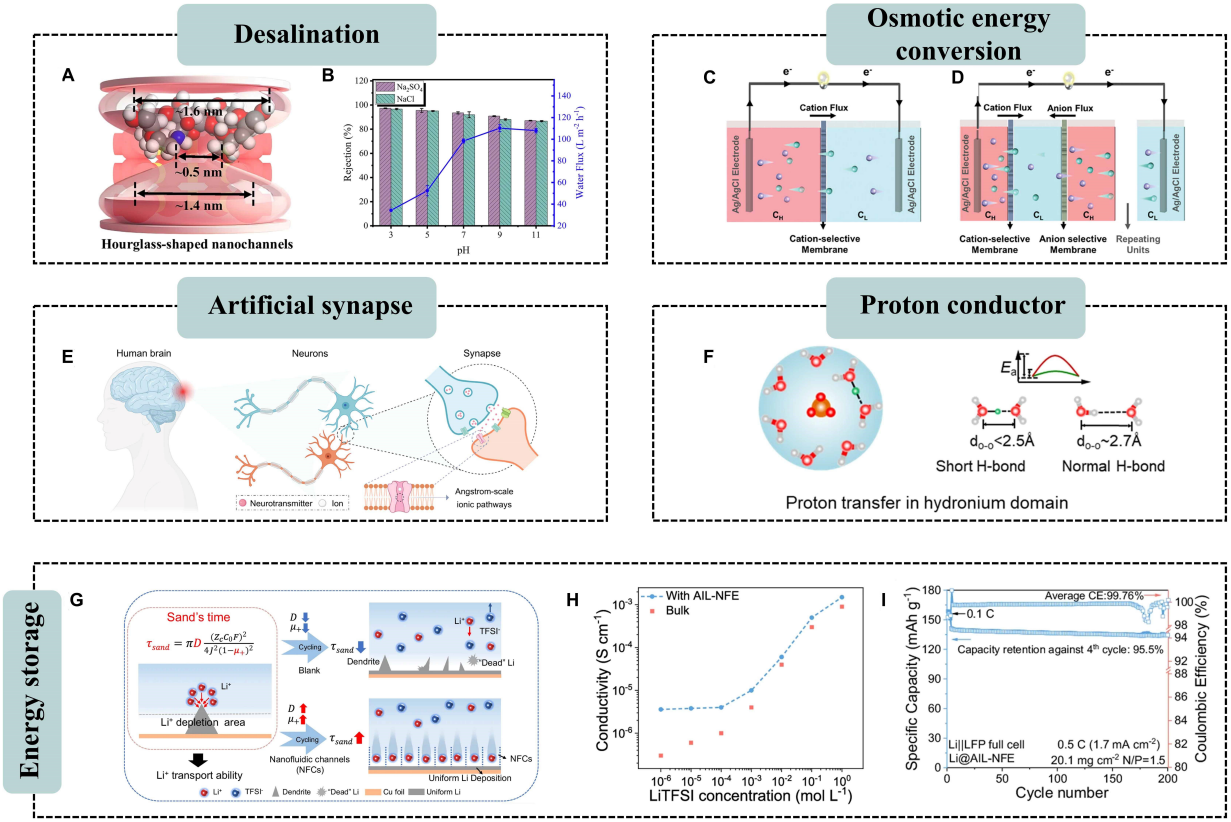

Figure 11. Applications of 2D organic framework membranes in desalination, osmotic energy conversion, artificial synapse, proton conductor and energy storage. (A) The illustration of hourglass-shaped nanochannels. (B) pH-dependent desalination performance of COF-CDN-12. (A and B) Ref.[182] Copyright © 2025, The Author(s); Osmotic energy device schematics: (C) half-cell and (D) full-cell. (C and D) Ref.[184] Copyright © 2024 The Author(s). Advanced Materials published by Wiley-VCH GmbH; (E) Schematic of ionic information processing in the human nervous system. (E) Ref.[9] Copyright © 2025, American Chemical Society; (F) Proton transport through SHB versus conventional H-bond within confined water. (F) Ref.[204] Copyright © 2022, The Author(s); (G-I) Li^+ transport/plating schematics, ionic conductivity, and cycling performance of Li@AIL-NFE||LFP cells[207]. (G-I) Reproduced under the CC-BY-NC license from Ref.[207] Copyright © 2025, The Author(s). LiTFSI: Lithium bis(trifluoromethanesulfonyl)imide; COF: covalent organic framework; CDN: cyclodextrin nanoparticle: Li@AIL-NFE||LFP: (AIL-NFE: artificial interphase layer inspired by the nanofluidic effects; LFP: lithium iron phosphate cathode; Li: lithium-metal anode).

device is depicted in Figure 11C and D[184]. Recent advances in 2D nanofluidic membranes, assembled to mimic biological ion channels with well-defined nanostructures, offer a potential solution. These membranes enable directional ion transport, significantly enhancing both selectivity and flux[110]. Two main types of membranes are used for this application: 2D laminar and single-layer membranes. Utilizing the tunability of 2D MOFs, Lin *et al.* developed an electrolyte-stable MXene/MOF (MXCT) membrane by alternately stacking $Ti_3C_2T_x$ and Cu-TCPP (Cu-tetrakis(4-carboxyphenyl)porphyrin) nanosheets[185]. The Cu-TCPP nanosheets featured sub-2 nm in-plane pores, which served as short and vertically oriented channels, whereas the MXene layers provided surface charges and hydrogen-bond cross-linking that prevented swelling and reduced resistance to 9 kΩ. Under a 50-fold NaCl gradient, this membrane generated electricity at a power density of 8.29 W/m², which was ~ 275% higher than pristine MXene[185]. The reported power output exceeded 49 W/m² at a 500-fold gradient, with stable Li^+ retention over seven days, providing a scalable route for ultralow-resistance blue energy harvesting[185].

Single-layer 2D membranes with atomic-scale nanopores exhibit extremely high permeability, making them ideal for reverse electrodialysis and desalination, as suggested by theory and experiment. Yang *et al.* scaled up COF synthesis to fabricate a free-standing monolayer membrane for macro-scale blue-energy harvesting[46]. Due to its high density of positively charged pores, the membrane demonstrates exceptional ion conductivity

and selectivity. Under a 50-fold NaCl concentration gradient, it achieves an osmotic power output of 135.8 W m^{-2}. This performance, thanks to the membrane's optimal thickness and high pore density, highlights a potential for low-resistance membrane applications.

Artificial synapse

Biological synapses are a basic element of biological neural networks, physically connecting two neurons and transmitting neuronal impulses. Synaptic plasticity refers to the ability of synapses to change the strength of their connections in response to activity patterns. This dynamic modulation, achieved through mechanisms such as long-term potentiation and depression, underpins learning, memory formation, and adaptive behavior in the brain. Memristors, whose resistance depends on the history of applied voltage or current, can be used to mimic synaptic plasticity. However, most of the state-of-the-art memristors are solid-state with electrons as the charge carriers. In contrast, nanofluidic memristors employ ions dissolved in water as charge carriers and exhibit nonlinear ion transport within highly confined spaces. This allows them to more faithfully replicate the ionic mechanisms and energy efficiency of biological synapses[186,187]. Unlike these efficient biological systems, conventional digital computers are based on the von Neumann architecture, which separates the central processing unit (CPU) from memory. This physical and functional separation creates the von Neumann bottleneck, in which processing speed is fundamentally limited by the constant need to shuttle data back and forth between memory and processor. With the rapidly growing demand for computational power in the AI era, overcoming this memory wall has become critical. Inspired by the low power consumption and high parallel computing of biological neural systems, nanofluidic memristive devices based on nanoconfined assembly and ions dissolved in water offer a bioinspired solution to push forward the physical limits of electronics by collocating memory and computing[188].

Nevertheless, achieving non-volatile memory in purely aqueous systems remains challenging due to the fast diffusion of ions. To overcome this, researchers introduced an immiscible KCl/ionic liquid (IL) interface into a nanochannel[189]. The voltage-induced displacement of this high-viscosity interface enables gradual and memorable tuning of conductance, successfully emulating synaptic weight changes with high accuracy. Beyond interfacial engineering, replicating the angstrom-scale thickness of biological ion channels is equally crucial [Figure 11E]. To reach this limit, atomically thin nanopores within 2D basal planes have been designed to decouple complex interaction processes, achieving synaptic emulation with ultralow energy consumption[9]. Specifically, the high porosity and abundant storage sites for ions in the basal planes of 2D organic frameworks could induce ionic memory effect, and therefore, they could serve as building blocks for the fabrication of nanofluidic memristors. Yu *et al.* developed nanofluidic synapses mimicking neurotransmitter-driven ion flux[190]. They utilized Cu-HITP (HITP = 2,3,6,7,10,11-hexaiminotriphenylene) and Cu-HHTP (HHTP = 2,3,6,7,10,11-hexahydroxytriphenylene) nanosheets for the fabrication due to their redox-active π-backbones and opposite surface charges. These nanosheets were stacked to form channels of less than 100 nm wide, where the pore walls acted as ion storage sites to produce hysteretic conductance, and also functioned as catalase-like centers that converted glutamate-produced H_2O_2 into O_2 and H_2O. Upon glutamate introduction, this enzymatic reaction generated a fast (millisecond-scale) ionic current, whose direction and magnitude were reversibly modulated by the MOF surface charge. This process allowed effective emulation of the nonlinear Hebbian and anti-Hebbian learning rules. By combining electrical programming with enzymatic glutamate clearance, the synaptic state was reset, thereby enabling reversible biochemical memory encoding at the single-channel level. This work bridges catalytic MOF chemistry with neuromorphic iontronics, paving the way for future electrolytic computing devices and brain-machine interfaces.

Proton conductor

Proton-conducting materials have attracted considerable interest in recent years. 2D crystals like graphene and hexagonal boron nitride (hBN) let thermal protons pass freely while completely blocking other ions and

gases[191,192]. However, practical applications require an areal conductivity exceeding 5 S cm^{-2}[193]. While inducing atomic defects or strain can improve performance, these structural modifications remain difficult to control precisely[192,194,195]. Additionally, operating in the "proton materials gap" (200-500 °C) is difficult for both 2D and 3D materials[196]. To solve this, 2D titania monolayers use a high density of intrinsic atomic vacancies to enable stable, fast proton transport at high temperatures[197]. Similarly, 2D organic frameworks utilize inherent sub-nanometer pathways to advance pore engineering. With customizable channels and functionalized hydrogen-bonding networks, these frameworks provide a precise platform to achieve both proton flux and ion selectivity[198,199].

Recently, spatial confinement of water molecules within laminated, porous architecture has attracted significant attention[200,201]. This creates a proton-rich local environment, increasing charge carrier concentration and accelerating water-mediated proton transfer, and hence, enabling the efficient development of high-performance proton-conducting materials[202,203]. Shi *et al.* used reticular chemistry to construct a densely packed, ordered array of -SO_3H ligands on crystalline ionic COF membranes (iCOFMs), anchoring a surface-confined short hydrogen-bond (SHB) network [Figure 11F][204]. By tuning the group distance from 2.5 to 0.8 nm, a limited number of surface water and hydronium per sulfonic acid group are confined, resulting in concentrated hydronium ions in water-hydronium domains (WHD, H_2O-H^+-OH_2)[204]. This network yields a record proton conductivity of 1.389 S cm^{-1} at 90 °C and 100% relative humidity, retaining 0.1 S cm^{-1} at 40% relative humidity. Combining humidity-resilient conductivity with the mechanical robustness of COFs, this approach offers a novel paradigm for advanced proton-exchange membranes.

Energy storage

The increasing demand for sustainable energy has intensified interest in Li^+ batteries, the leading technology for portable power due to their high energy density and long cycle life[205]. Integrating 2D organic framework membranes into anodes, separators, and cathodes facilitates rapid, selective Li^+ transport, provides abundant surface storage sites, and enhances mechanical robustness, collectively improving cycling stability[206].

For lithium-metal anodes, suppressing dendrite requires preventing interfacial Li^+ depletion. To this end, an artificial interphase layer emulating biological nanofluidic channels (AIL-NFE) was developed using 4-carboxyl-quinoline-linked COFs [Figure 11G][207]. Its aligned nanofluidic confinement delivered a Li^+ conductivity of ~ 0.1 mS cm^{-1} at salt concentrations ≤ 10^{-4} mol L^{-1} [Figure 11H]. The selective, rapid Li^+ conduction gave rise to a uniform interfacial ion flux, enabling dendrite-free lithium plating and stripping at 50 mA cm^{-2} for over 1,000 h. Moreover, Li@AIL-NFE||LFP (AIL-NFE: artificial interphase layer inspired by the nanofluidic effects; LFP: lithium iron phosphate cathode; Li: lithium metal anode) cells achieved 95.5% coulombic efficiency after 200 cycles [Figure 11I]. These results highlight the potential of nature-inspired nanofluidic interfaces for high-rate, stable lithium-metal batteries.

2D membranes have garnered significant attention as advanced separators, owing to their high surface charge and ion selectivity. They effectively mitigate polysulfide shuttling, a key challenge in lithium-sulfur (Li-S) batteries. For example, Bai *et al.* developed a MOF@GO composite separator to mitigate the shuttle effect of polysulfide, a key challenge in Li-S batteries[208]. Acting as an ionic sieve, the MOF@GO membrane selectively permitted Li^+ transport while blocking polysulfide migration to the anode. Compared to a pure GO separator, it offered superior polysulfide blocking, significantly enhanced cycling stability and a rate performance at 1 C over 1,500 cycles[208].

On the other hand, an ion-gated coating layer employing nanofluidic effects observed in biological systems (IGCL-NFE) was developed to facilitate ultrafast and selective Li^+ transport while inhibiting polysulfide shuttling. Song *et al.* constructed the IGCL-NFE using 4-carboxyl-quinoline-linked COFs in the sulfur

cathode[209]. This biomimetic interface achieved a Li^+ transference number (μ_+) ~ 2.1 times higher and a diffusion coefficient (D_{Li+}) ~ 10^{12} times greater than conventional bulk electrolytes at 10^{-6} mol L^{-1} LiTFSI, while preventing lithium polysulfide migration. The conductive coating (0.38 S cm^{-1}) featured a nanoconfined architecture that shortened electron and ion transport pathways in thick electrodes, thereby reducing charge-transfer resistance. This maintained a capacity of 757.8 mAh g^{-1} after 300 cycles at 10 C (16.7 mA cm^{-2}), providing a viable strategy for ultrahigh-loading, high-rate Li-S batteries.

CONCLUSION AND OUTLOOK

Over the past two decades, nanofluidics has evolved from the first nano-hole drilled in silicon nitride to applications in biopolymer sequencing, filtration, energy harvesting, energy storage, and neuromorphic logic circuits. In this Review, we have summarized recent progress in 2D organic framework membranes, covering their structures, properties, composition, and nanofluidics-related applications. Nonetheless, significant challenges remain before their real applications.

A key challenge is to understand ion transport mechanisms across macroscopic, nanoscopic, and angstrom scales, which is fundamental in both membrane science and nanofluidics[210]. While theoretical models like Debye overlap explain selective transport in simplified systems very well, their applicability to complex organic framework nanofluidic systems requires reassessment. Real-world systems involve structural complexities and intricate ionic interactions that go beyond the assumptions of simplified models. Moreover, it remains uncertain whether single-channel mechanisms hold for large-area multichannel membranes. To resolve these uncertainties, researchers must rely on advanced characterization tools with high spatial and temporal resolutions. For example, using time-resolved *in situ* X-ray techniques can directly map double-layer structures within confined spaces[211,212]. Furthermore, coupling nanofluidic channels with diverse electrochemical probes precisely tracks confined ion fluxes via electrochemical quartz crystal microbalances (EQCM)[213].

In addition to these theoretical uncertainties, practical experimental challenges also remain, particularly those related to the wetting of membrane's surface and bubble formation in the fluidic path. Trapped nanoscale bubbles can obstruct fluidic pathways and prevent conduction. Activation strategies include prolonged water storage to dissipate bubbles or ethanol prewetting to enhance wettability[214]. In addition, thermal annealing is highly effective. Thermal annealing at 300 to 350 °C for 2 to 3 h under an Ar/H_2 (9:1) atmosphere reliably reduces bubble areas by over 80%[215]. Thus, early-stage nonlinearities should be interpreted with extreme care, as they may reflect transient bubble dynamics rather than intrinsic material or interfacial properties. Preventing bubble reformation during prolonged operation is also crucial for experimental reproducibility.

The ultrafast transport in biological ion channels, unexplained by classical thermodynamics, continues to inspire artificial nanofluidic systems. However, engineering 2D membranes that truly mimic biological counterparts remains difficult. Recent advances in the science of 2D organic framework materials offer avenues for sophisticated, structurally controllable nanofluidic membranes[216]. Their tunable pores and surface functionalities provide ideal platforms for studying nanofluidics. Nonetheless, scalable production faces difficulties including stringent processing, purification, and the need for defect-free, long-range ordered macroscopic materials. Additionally, directly observing ion dynamics within individual nanochannels is extremely challenging. While molecular dynamics simulations have quantitatively revealed ion transport mechanisms, experiments for real-space visualization are needed[93]. Advancing super-resolution optical methods is promising. Specifically, a recent study employed optical imaging to map proton transport on hBN surfaces in an aqueous environment, which demonstrated the potential for spatiotemporal tracking of ion dynamics[217]. Moreover, performance metrics for novel 2D materials may be overestimated if tested on

excessively small areas. For instance, reported ultra-high osmotic energy conversion efficiencies are often limited to small active areas[49]. Similarly, conventional selectivity assessments often rely solely on sieving, offering only a partial understanding of separation mechanisms.

Despite the described challenges, abundant opportunities are also present. 2D organic framework membranes offer vast opportunities for nanofluidics. As a rapidly evolving field, nanofluidics remains largely unexplored in many aspects. Although ion transport is inherently slower than electron conduction, ions possess unique advantages due to their diverse valence states, sizes, and polarizabilities. In this regard, one of the promising future research directions is to emulate neural signaling mechanisms of the human brain through artificial nanofluidic device platforms[218]. Such systems are promising for artificial intelligence, brain-machine interfaces, and brain-inspired computing. These emerging research fields present fundamental scientific challenges in physics and chemistry (of course), while offering transformative opportunities to address critical societal issues[219].

DECLARATIONS

Authors' contributions

Conceptualization and writing: Cui, H.; Wang, D. W.; Sun, P.
Supervision: Wang, D.W.; Sun, P.
Made substantial contributions to revising the manuscript: Ji, Y.; Chen, K.; Zhou, W.; Lin, Q.; Yin, Z.; Lin, L.

Availability of data and materials

Not applicable.

AI and AI-assisted tools statement

Not applicable.

Financial support and sponsorship

Lin, L. acknowledges support from the National Key Research and Development Program of China (2024YFE0202200). Sun, P. acknowledges support from the Natural Science Foundation of China (52322319), the Science and Technology Development Fund, Macao SAR (0063/2023/RIA1, 0107/2024/AMJ), UM research grant (MYRG-GRG2025-00006-IAPME, MYRG-CRG2024-00012-IAPME, MYRG-GRG2024-00064-IAPME). Wang, D.W. acknowledges support from the Guangdong Pearl River Talent Program of China (2023ZT10L045).

Conflicts of interest

Sun, P. is an Editorial Board Member of *Iontronics* and a Guest Editor of the Special Issue, "Fundamental Understanding and Applications of Molecular and Ionic Transport through (Sub)Nanometer-Scale Pores or Channels Made by 2D Materials," in *Iontronics*. He is not involved in any steps of editorial processing, notably including reviewers' selection, manuscript handling, or decision-making. The other authors declare that they have no conflicts of interest.

Ethical approval and consent to participate

Not applicable.

Consent for publication

Not applicable.

REFERENCES

1. Schroeder, T. B. H.; Guha, A.; Lamoureux, A.; et al. An electric-eel-inspired soft power source from stacked hydrogels. *Nature* **2017**, *552*, 214-8. DOI PubMed PMC

2. Kato, H. E.; Kim, Y. S.; Paggi, J. M.; et al. Structural mechanisms of selectivity and gating in anion channelrhodopsins. *Nature* **2018**, *561*, 349-54. DOI PubMed PMC
3. Ruan, Z.; Osei-Owusu, J.; Du, J.; Qiu, Z.; Lü, W. Structures and pH-sensing mechanism of the proton-activated chloride channel. *Nature* **2020**, *588*, 350-4. DOI PubMed PMC
4. Kopec, W.; Köpfer, D. A.; Vickery, O. N.; et al. Direct knock-on of desolvated ions governs strict ion selectivity in K^+ channels. *Nature. Chem.* **2018**, *10*, 813-20. DOI
5. Noskov, S. Y.; Bernèche, S.; Roux, B. Control of ion selectivity in potassium channels by electrostatic and dynamic properties of carbonyl ligands. *Nature* **2004**, *431*, 830-4. DOI
6. Liao, X.; Song, W.; Zhang, X.; et al. A bioinspired analogous nerve towards artificial intelligence. *Nat. Commun.* **2020**, *11*, 268. DOI PubMed PMC
7. Bocquet, L. Nanofluidics coming of age. *Nat. Mater.* **2020**, *19*, 254-6. DOI
8. Tan, R.; Wang, A.; Malpass-Evans, R.; et al. Hydrophilic microporous membranes for selective ion separation and flow-battery energy storage. *Nat. Mater.* **2020**, *19*, 195-202. DOI
9. Song, R.; Wang, P.; Zeng, H.; et al. Nanofluidic memristive transition and synaptic emulation in atomically thin pores. *Nano. Lett.* **2025**, *25*, 5646-55. DOI
10. Laucirica, G.; Toum-Terrones, Y.; Cayón, V. M.; Toimil-Molares, M. E.; Azzaroni, O.; Marmisollé, W. A. Advances in nanofluidic field-effect transistors: external voltage-controlled solid-state nanochannels for stimulus-responsive ion transport and beyond. *Phys. Chem. Chem. Phys.* **2024**, *26*, 10471-93. DOI
11. Raidongia, K.; Huang, J. Nanofluidic ion transport through reconstructed layered materials. *J. Am. Chem. Soc.* **2012**, *134*, 16528-31. DOI
12. Tang, J.; Wang, Y.; Yang, H.; et al. All-natural 2D nanofluidics as highly-efficient osmotic energy generators. *Nat. Commun.* **2024**, *15*, 3649. DOI PubMed PMC
13. Zhang, H.; Yong, M.; Hu, T.; et al. Multifunctional intercalants create stable subnanochannels in MoS_2 membranes for wastewater treatment. *Nat. Commun.* **2025**, *16*, 8353. DOI
14. Macha, M.; Marion, S.; Nandigana, V. V. R.; Radenovic, A. 2D materials as an emerging platform for nanopore-based power generation. *Nat. Rev. Mater.* **2019**, *4*, 588-605. DOI
15. Zhou, T.; Cheng, Q. Chemical strategies for making strong graphene materials. *Angew. Chem.* **2021**, *133*, 18545-58. DOI
16. Liu, M.; Weston, P. J.; Hurt, R. H. Controlling nanochannel orientation and dimensions in graphene-based nanofluidic membranes. *Nat. Commun.* **2021**, *12*, 507. DOI PubMed PMC
17. Serrano-plana, J. A framework for chemists. *Nature. Chem.* **2025**, *17*, 1802. DOI
18. Qian, C.; Zhao, X. two-dimensional heteropore covalent organic frameworks: from construction to functions. *Acc. Chem. Res.* **2025**, *58*, 1192-209. DOI
19. Chen, Z.; Li, C.; Ge, Z.; Wu, S.; Liang, B.; Bu, X. Crystalline porous membrane devices: emerging architectures for carbon-neutral technologies. *Mater. Horiz.* **2025**, *12*, 7101-32. DOI
20. Wang, Y.; Hu, Y.; Guo, J.; Gao, J.; Song, B.; Jiang, L. A physical derivation of high-flux ion transport in biological channel via quantum ion coherence. *Nat. Commun.* **2024**, *15*, 7189. DOI
21. Gadsby, D. C. Ion channels versus ion pumps: the principal difference, in principle. *Nat. Rev. Mol. Cell. Biol.* **2009**, *10*, 344-52. DOI PubMed PMC
22. Roux, B. Computational studies of the gramicidin channel. *Acc. Chem. Res.* **2002**, *35*, 366-75. DOI
23. Yan, Z.; Zhou, Q.; Wang, L.; et al. Structure of the Nav1.4-β1 complex from electric eel. *Cell* **2017**, *170*, 470-482.e11. DOI
24. Dang, S.; Feng, S.; Tien, J.; et al. Cryo-EM structures of the TMEM16A calcium-activated chloride channel. *Nature* **2017**, *552*, 426-9. DOI PubMed PMC
25. Basu, D.; Haswell, E. S. The mechanosensitive ion channel MSL10 potentiates responses to cell swelling in Arabidopsis seedlings. *Curr. Biol.* **2020**, *30*, 2716-2728.e6. DOI
26. Xu, J.; Tang, F. Voltage-dependent calcium channels, calcium binding proteins, and their interaction in the pathological process of epilepsy. *Int. J. Mol. Sci.* **2018**, *19*, 2735. DOI PubMed PMC
27. Sanz, A.; Pike, S.; Khan, M. A.; et al. Copper uptake mechanism of Arabidopsis thaliana high-affinity COPT transporters. *Protoplasma* **2019**, *256*, 161-70. DOI
28. Zakeri, B.; Fierer, J. O.; Celik, E.; et al. Peptide tag forming a rapid covalent bond to a protein, through engineering a bacterial adhesin. *Proc. Natl. Acad. Sci. U.S.A.* **2012**, *109*. DOI PubMed PMC
29. Robin, P.; Kavokine, N.; Bocquet, L. Modeling of emergent memory and voltage spiking in ionic transport through angstrom-scale slits. *Science* **2021**, *373*, 687-91. DOI
30. Hodgkin, A. L.; Huxley, A. F. A quantitative description of membrane current and its application to conduction and excitation in nerve. *J. Physiol.* **1952**, *117*, 500-44. DOI PubMed PMC

31. Moujahid, A.; D'Anjou, A. Metabolic efficiency with fast spiking in the squid axon. *Front. Comput. Neurosci.* **2012**, *6*, 95. DOI PubMed PMC
32. Hille, B. Ionic channels in nerve membranes, 50 years on. *Prog. Biophys. Mol. Biol.* **2022**, *169-170*, 12-20. DOI PubMed PMC
33. Doyle, D. A.; Cabral, J. M.; Pfuetzner, R. A.; et al. The structure of the potassium channel: molecular basis of K^+ conduction and selectivity. *Science* **1998**, *280*, 69-77. DOI
34. Tempel, B. L.; Papazian, D. M.; Schwarz, T. L.; Jan, Y. N.; Jan, L. Y. Sequence of a probable potassium channel component encoded at *Shaker* locus of *Drosophila*. *Science* **1987**, *237*, 770-5. DOI
35. Li, J.; Stein, D.; Mcmullan, C.; Branton, D.; Aziz, M. J.; Golovchenko, J. A. Ion-beam sculpting at nanometre length scales. *Nature* **2001**, *412*, 166-9. DOI
36. Wang, M.; Hou, Y.; Yu, L.; Hou, X. Anomalies of ionic/molecular transport in nano and sub-nano confinement. *Nano. Lett.* **2020**, *20*, 6937-46. DOI
37. Novoselov, K. S.; Geim, A. K.; Morozov, S. V.; et al. Electric field effect in atomically thin carbon films. *Science* **2004**, *306*, 666-9. DOI
38. Surwade, S. P.; Smirnov, S. N.; Vlassiouk, I. V.; et al. Water desalination using nanoporous single-layer graphene. *Nat. Nanotechnol.* **2015**, *10*, 459-64. DOI
39. Heiranian, M.; Farimani, A. B.; Aluru, N. R. Water desalination with a single-layer MoS_2 nanopore. *Nat. Commun.* **2015**, *6*, 8616. DOI
40. Nair, R. R.; Wu, H. A.; Jayaram, P. N.; Grigorieva, I. V.; Geim, A. K. Unimpeded permeation of water through helium-leak-tight graphene-based membranes. *Science* **2012**, *335*, 442-4. DOI
41. Bunck, D. N.; Dichtel, W. R. Bulk synthesis of exfoliated two-dimensional polymers using hydrazone-linked covalent organic frameworks. *J. Am. Chem. Soc.* **2013**, *135*, 14952-5. DOI
42. Jung, M.; Kim, H.; Baek, K.; Kim, K. Synthetic ion channel based on metal-organic polyhedra. *Angew. Chem. Int. Ed.* **2008**, *47*, 5755-7. DOI
43. Zhang, H.; Hou, J.; Hu, Y.; et al. Ultrafast selective transport of alkali metal ions in metal organic frameworks with subnanometer pores. *Sci. Adv.* **2018**, *4*, eaaq0066. DOI PubMed PMC
44. Zhang, P.; Chen, S.; Zhu, C.; et al. Covalent organic framework nanofluidic membrane as a platform for highly sensitive bionic thermosensation. *Nat. Commun.* **2021**, *12*, 1844. DOI PubMed PMC
45. Bing, S.; Xian, W.; Chen, S.; et al. Bio-inspired construction of ion conductive pathway in covalent organic framework membranes for efficient lithium extraction. *Matter* **2021**, *4*, 2027-38. DOI
46. Yang, J.; Tu, B.; Zhang, G.; et al. Advancing osmotic power generation by covalent organic framework monolayer. *Nat. Nanotechnol.* **2022**, *17*, 622-8. DOI
47. Zuo, P.; Ye, C.; Jiao, Z.; et al. Near-frictionless ion transport within triazine framework membranes. *Nature* **2023**, *617*, 299-305. DOI PubMed PMC
48. Xu, T.; Wu, B.; Li, W.; et al. Perfect confinement of crown ethers in MOF membrane for complete dehydration and fast transport of monovalent ions. *Sci. Adv.* **2024**, *10*, eadn0944. DOI PubMed PMC
49. Zhang, Z.; Wen, L.; Jiang, L. Nanofluidics for osmotic energy conversion. *Nat. Rev. Mater.* **2021**, *6*, 622-39. DOI
50. Xu, Q.; Tao, S.; Jiang, Q.; Jiang, D. Designing covalent organic frameworks with a tailored ionic interface for ion transport across one-dimensional channels. *Angew. Chem.* **2020**, *132*, 4587-93. DOI
51. Gou, F.; Yao, Y.; Wang, Q.; et al. Flexible crown-ether polyimides break the K^+/Na^+ selectivity barrier in artificial K^+ channels. *Angew. Chem.* **2026**, *138*, e20146. DOI
52. Sun, Q.; Dou, P.; Du, J.; et al. Biomimetic KcsA channels enabled by 1D MOF-in-2D COF. *Nat. Commun.* **2025**, *16*, 9099. DOI PubMed PMC
53. Kong, Y.; Lyu, B.; Fan, C.; et al. Manipulation of cationic group density in covalent organic framework membranes for efficient anion transport. *J. Am. Chem. Soc.* **2023**, *145*, 27984-92. DOI
54. Mous, S.; Gotthard, G.; Ehrenberg, D.; et al. Dynamics and mechanism of a light-driven chloride pump. *Science* **2022**, *375*, 845-51. DOI
55. Zhou, Y.; Xiong, T.; Lu, J.; et al. Highly-efficient ion gating through self-assembled two-dimensional photothermal metal-organic framework membrane. *Angew. Chem. Int. Ed.* **2023**, *62*, e202302997. DOI
56. Lei, D.; Zhang, Q.; Wang, Y.; et al. Nature-inspired solid-state proton diode membrane for high-performance force-electric conversion. *Nat. Commun.* **2026**, *17*, 3138. DOI PubMed PMC
57. Wang, H.; Zhang, Y.; Wang, J.; et al. *In situ* synthesized HOF ion rectification membrane with ultrahigh permselectivity for nanofluidic osmotic energy harvesting. *Adv. Funct. Mater.* **2025**, *35*, 2412477. DOI
58. Wang, M.; Xiong, Q.; Yue, X.; et al. Cooperative and inhibitory ion transport in functionalized angstrom-scale two-dimensional channels. *Nat. Commun.* **2025**, *16*, 5854. DOI PubMed PMC

59. Enke, U.; Schweinitz, A.; Tewari, D.; et al. HCN1 is a primary HCN pacemaker channel in neurons. *Nat. Commun.* **2026**, *17*, 3745. DOI PubMed PMC
60. Wang, J.; Zhang, J.; Jin, P.; et al. A covalent organic framework membrane with highly selective and permeable artificial sodium channels via ion recognition. *Nat. Commun.* **2025**, *16*, 7346. DOI PubMed PMC
61. Xue, Y.; Xia, Y.; Yang, S.; et al. Atomic-scale ion transistor with ultrahigh diffusivity. *Science* **2021**, *372*, 501-3. DOI
62. Epsztein, R.; Duchanois, R. M.; Ritt, C. L.; Noy, A.; Elimelech, M. Towards single-species selectivity of membranes with subnanometre pores. *Nat. Nanotechnol.* **2020**, *15*, 426-36. DOI
63. Gao, J.; Feng, Y.; Guo, W.; Jiang, L. Nanofluidics in two-dimensional layered materials: inspirations from nature. *Chem. Soc. Rev.* **2017**, *46*, 5400-24. DOI
64. Yu, X.; Ren, W. Ion and water transport in 2D nanofluidic channels. *Adv. Funct. Mater.* **2024**, *34*, 2313968. DOI
65. Vlassiouk, I.; Smirnov, S.; Siwy, Z. Ionic selectivity of single nanochannels. *Nano. Lett.* **2008**, *8*, 1978-85. DOI
66. Zhang, X.; Song, B.; Jiang, L. Driving force of molecular/ionic superfluid formation. *CCS. Chem.* **2021**, *3*, 1258-66. DOI
67. Zhou, K.; Xu, Z. Ion permeability and selectivity in composite nanochannels: engineering through the end effects. *J. Phys. Chem. C.* **2020**, *124*, 4890-8. DOI
68. Lai, Z.; Ai, Y.; Xian, W.; et al. Covalent-organic-framework membrane with aligned dipole moieties for biomimetic regulable ion transport. *Adv. Funct. Mater.* **2024**, *34*, 2409356. DOI
69. Schoch, R. B.; Han, J.; Renaud, P. Transport phenomena in nanofluidics. *Rev. Mod. Phys.* **2008**, *80*, 839-83. DOI
70. Bocquet, L.; Charlaix, E. Nanofluidics, from bulk to interfaces. *Chem. Soc. Rev.* **2010**, *39*, 1073-95. DOI
71. Zhang, W.; Zhang, A.; Zhou, W.; Ji, Y.; Xu, Z.; Sun, P. Revisiting ion transport through micropores: significant and non-negligible surface transport. *Nanoscale. Horiz.* **2026**, *11*, 795-802. DOI
72. Chen, L.; Tu, B.; Lu, X.; et al. Unidirectional ion transport in nanoporous carbon membranes with a hierarchical pore architecture. *Nat. Commun.* **2021**, *12*, 4650. DOI PubMed PMC
73. Esfandiar, A.; Radha, B.; Wang, F. C.; et al. Size effect in ion transport through angstrom-scale slits. *Science* **2017**, *358*, 511-3. DOI
74. Richards, L. A.; Schäfer, A. I.; Richards, B. S.; Corry, B. The importance of dehydration in determining ion transport in narrow pores. *Small* **2012**, *8*, 1701-9. DOI
75. Sahu, S.; Di Ventra, M.; Zwolak, M. Dehydration as a universal mechanism for ion selectivity in graphene and other atomically thin pores. *Nano. Lett.* **2017**, *17*, 4719-24. DOI PubMed PMC
76. Rollings, R. C.; Kuan, A. T.; Golovchenko, J. A. Ion selectivity of graphene nanopores. *Nat. Commun.* **2016**, *7*, 11408. DOI
77. Alibakhshi, M. A.; Kang, X.; Clymer, D.; et al. Scaled-up synthesis of freestanding molybdenum disulfide membranes for nanopore sensing. *Adv. Mater.* **2023**, *35*, 2207089. DOI
78. Cao, Z.; Liu, V.; Barati Farimani, A. Why is single-layer MoS_2 a more energy efficient membrane for water desalination? *ACS. Energy. Lett.* **2020**, *5*, 2217-22. DOI
79. Lee, M. K.; Shokouhimehr, M.; Kim, S. Y.; Jang, H. W. Two-dimensional metal-organic frameworks and covalent-organic frameworks for electrocatalysis: distinct merits by the reduced dimension. *Adv. Energy. Mater.* **2022**, *12*, 2003990. DOI
80. Chen, X.; Zhang, H.; Liu, S.; Zhou, Y.; Jiang, L. Engineering polymeric nanofluidic membranes for efficient ionic transport: biomimetic design, material construction, and advanced functionalities. *ACS. Nano.* **2022**, *16*, 17613-40. DOI
81. Mo, R.; Chen, S.; Huang, L.; et al. Regulating ion affinity and dehydration of metal-organic framework sub-nanochannels for high-precision ion separation. *Nat. Commun.* **2024**, *15*, 2145. DOI
82. Zhang, Z.; Shen, W.; Lin, L.; et al. Vertically transported graphene oxide for high-performance osmotic energy conversion. *Adv. Sci.* **2020**, *7*, 2000286. DOI
83. Lan, X.; Li, Z.; Zhao, C.; et al. Superionic composite electrolytes with continuously perpendicular-aligned pathways for pressure-less all-solid-state lithium batteries. *Nat. Nanotechnol.* **2026**, *21*, 388-96. DOI
84. Wang, S.; Yang, L.; He, G.; et al. Two-dimensional nanochannel membranes for molecular and ionic separations. *Chem. Soc. Rev.* **2020**, *49*, 1071-89. DOI
85. Naren, T.; Gu, Q.; Jiang, R.; et al. Nanoconfined polymerization facilitates efficient Li^+ transportation in quasi-solid electrolytes. *Angew. Chem. Int. Ed.* **2025**, *64*, e202509921. DOI
86. Gong, Y.; Sun, P.; Ji, Y. Atomically thin sieves: two-dimensional materials for membrane separation. *Adv. Phys. Res.* **2026**, *5*, e00183. DOI
87. Kim, S.; Choi, H.; Kim, B.; et al. Extreme ion-transport inorganic 2D membranes for nanofluidic applications. *Adv. Mater.* **2023**, *35*, 2206354. DOI
88. Corry, B. Designing carbon nanotube membranes for efficient water desalination. *J. Phys. Chem. B.* **2008**, *112*, 1427-34. DOI
89. Konatham, D.; Yu, J.; Ho, T. A.; Striolo, A. Simulation insights for graphene-based water desalination membranes. *Langmuir* **2013**, *29*, 11884-97. DOI

90. Zhao, S.; Xue, J.; Kang, W. Ion selection of charge-modified large nanopores in a graphene sheet. *J. Chem. Phys.* **2013**, *139*, 114702. DOI
91. Suk, M. E.; Aluru, N. R. Ion transport in sub-5-nm graphene nanopores. *J. Chem. Phys.* **2014**, *140*, 084707. DOI
92. Wang, L.; Boutilier, M. S. H.; Kidambi, P. R.; Jang, D.; Hadjiconstantinou, N. G.; Karnik, R. Fundamental transport mechanisms, fabrication and potential applications of nanoporous atomically thin membranes. *Nat. Nanotechnol.* **2017**, *12*, 509-22. DOI
93. Liao, S.; Liu, Y.; Li, L.; Ding, L.; Wei, Y.; Wang, H. Theoretical framework for confined ion transport in two-dimensional nanochannels. *Nat. Commun.* **2025**, *16*, 6675. DOI
94. Robin, P.; Emmerich, T.; Ismail, A.; et al. Long-term memory and synapse-like dynamics in two-dimensional nanofluidic channels. *Science* **2023**, *379*, 161-7. DOI
95. Matile, S., Sakai, N., Hennig, A. Transport experiments in membranes. In *Supramolecular chemistry*; Gale, P. A., Steed, J. W., Eds.; Wiley, 2012. DOI
96. Rideau, E.; Dimova, R.; Schwille, P.; Wurm, F. R.; Landfester, K. Liposomes and polymersomes: a comparative review towards cell mimicking. *Chem. Soc. Rev.* **2018**, *47*, 8572-610. DOI
97. Valkenier, H.; López mora, N.; Kros, A.; Davis, A. P. Visualization and quantification of transmembrane ion transport into giant unilamellar vesicles. *Angew. Chem. Int. Ed.* **2015**, *54*, 2137-41. DOI
98. Shen, J.; R, D.; Li, Z.; et al. Sulfur-containing foldamer-based artificial lithium channels. *Angew. Chem. Int. Ed.* **2023**, *62*, e202305623. DOI
99. Wu, B.; Yan, Y.; Zhu, Y.; Ji, C.; Lin, Y.; Lang, C. Ions in motion: from biological channels to engineered transport systems. *Giant* **2025**, *22*, 100352. DOI
100. Ren, C.; Zeng, F.; Shen, J.; et al. Pore-forming monopeptides as exceptionally active anion channels. *J. Am. Chem. Soc.* **2018**, *140*, 8817-26. DOI
101. Lee, C.; Joly, L.; Siria, A.; Biance, A.; Fulcrand, R.; Bocquet, L. Large apparent electric size of solid-state nanopores due to spatially extended surface conduction. *Nano. Lett.* **2012**, *12*, 4037-44. DOI
102. Sheng, Q.; Xie, Y.; Li, J.; Wang, X.; Xue, J. Transporting an ionic-liquid/water mixture in a conical nanochannel: a nanofluidic memristor. *Chem. Commun.* **2017**, *53*, 6125-7. DOI
103. Siria, A.; Poncharal, P.; Biance, A.; et al. Giant osmotic energy conversion measured in a single transmembrane boron nitride nanotube. *Nature* **2013**, *494*, 455-8. DOI
104. Emmerich, T.; Teng, Y.; Ronceray, N.; et al. Nanofluidic logic with mechano-ionic memristive switches. *Nat. Electron.* **2024**, *7*, 271-8. DOI
105. Soni, N.; Chandra Verma, N.; Talor, N.; Meller, A. Over 30-fold enhancement in DNA translocation dynamics through nanoscale pores coated with an anionic surfactant. *Nano. Lett.* **2023**, *23*, 4609-16. DOI
106. Zhao, K.; Lee, W.; Rezaei, M.; et al. Tuning pore size in graphene in the angstrom regime for highly selective ion-ion separation. *ACS. Nano.* **2024**, acsnano.3c11068. DOI
107. Sorgato, M. C.; Keller, B. U.; Stühmer, W. Patch-clamping of the inner mitochondrial membrane reveals a voltage-dependent ion channel. *Nature* **1987**, *330*, 498-500. DOI
108. Kodirov, S. A. Whole-cell patch-clamp recording and parameters. *Biophys. Rev.* **2023**, *15*, 257-88. DOI
109. Maher, J.; Allen, M. Planar lipid bilayers in recombinant ion channel research. *Methods* **2018**, *147*, 206-12. DOI
110. Luo, J.; Qiao, R.; Ding, B. Enhancement of ion selectivity and permeability in two-dimensional material membranes. *Matter* **2024**, *7*, 3351-89. DOI
111. Wang, D.; Li, J.; Chen, B. Reticular design of hydrogen-bonded organic frameworks (HOFs): from structure tuning to function customization. *Angew. Chem. Int. Ed.* **2026**, *65*, e8641245. DOI
112. Jiang, H.; Alezi, D.; Eddaoudi, M. A reticular chemistry guide for the design of periodic solids. *Nat. Rev. Mater.* **2021**, *6*, 466-87. DOI
113. Lu, L.; Li, L.; Chu, M.; et al. Recent Advancement in 2D metal-organic framework for environmental remediation: a review. *Adv. Funct. Mater.* **2025**, *35*, 2419433. DOI
114. Zheng, Y.; Sun, F. Z.; Han, X.; Xu, J.; Bu, X. H. Recent progress in 2D metal-organic frameworks for optical applications. *Adv. Opt. Mater.* **2020**, *8*, 2000110. DOI
115. Zhang, Y.; Yang, L.; Yang, Y.; et al. Bidirectional light-driven ion transport through porphyrin metal-organic framework-based van der Waals heterostructures via pH-induced band alignment inversion. *CCS. Chem.* **2022**, *4*, 3329-41. DOI
116. Maeda, H.; Sakamoto, R.; Nishihara, H. Coordination programming of two-dimensional metal complex frameworks. *Langmuir* **2016**, *32*, 2527-38. DOI
117. Dou, J.; Sun, L.; Ge, Y.; et al. Signature of metallic behavior in the metal-organic frameworks M_3(hexaiminobenzene)$_2$ (M = Ni, Cu). *J. Am. Chem. Soc.* **2017**, *139*, 13608-11. DOI

118. Roh, H.; Su, A. Y.; Oh, C.; et al. Turning 2D MOFs into mixed ionic-electronic conductors via side chain engineering. *J. Am. Chem. Soc.* **2025**, *147*, 38419-27. DOI
119. Liang, R.; Jiang, S.; A, R.; Zhao, X. Two-dimensional covalent organic frameworks with hierarchical porosity. *Chem. Soc. Rev.* **2020**, *49*, 3920-51. DOI
120. Li, J.; Zhou, X.; Wang, J.; Li, X. Two-dimensional covalent organic frameworks (COFs) for membrane separation: a mini review. *Ind. Eng. Chem. Res.* **2019**, *58*, 15394-406. DOI
121. Geng, K.; He, T.; Liu, R.; et al. Covalent organic frameworks: design, synthesis, and functions. *Chem. Rev.* **2020**, *120*, 8814-933. DOI
122. Cao, L.; Liu, X.; Shinde, D. B.; et al. Oriented two-dimensional covalent organic framework membranes with high ion flux and smart gating nanofluidic transport. *Angew. Chem.* **2022**, *134*, e202113141. DOI
123. Yin, Q.; Zhao, P.; Sa, R. J.; et al. An ultra-robust and crystalline redeemable hydrogen-bonded organic framework for synergistic chemo-photodynamic therapy. *Angew. Chem.* **2018**, *130*, 7817-22. DOI
124. Karmakar, A.; Illathvalappil, R.; Anothumakkool, B.; et al. Hydrogen-bonded organic frameworks (HOFs): a new class of porous crystalline proton-conducting materials. *Angew. Chem. Int. Ed.* **2016**, *55*, 10667-71. DOI
125. Song, X.; Wang, Y.; Wang, C.; et al. Design rules of hydrogen-bonded organic frameworks with high chemical and thermal stabilities. *J. Am. Chem. Soc.* **2022**, *144*, 10663-87. DOI
126. Lin, Z.; Qin, J.; Zhan, X.; Wu, K.; Cao, G.; Chen, B. Robust mesoporous functional hydrogen-bonded organic framework for hypochlorite detection. *ACS. Appl. Mater. Interfaces.* **2022**, *14*, 21098-105. DOI
127. Lin, Z.; Mahammed, S. A. R.; Liu, T.; Cao, R. Multifunctional porous hydrogen-bonded organic frameworks: current status and future perspectives. *ACS. Cent. Sci.* **2022**, *8*, 1589-608. DOI
128. Zhou, H.; Long, J. R.; Yaghi, O. M. Introduction to metal-organic frameworks. *Chem. Rev.* **2012**, *112*, 673-4. DOI
129. Huang, N.; Wang, P.; Jiang, D. Covalent organic frameworks: a materials platform for structural and functional designs. *Nat. Rev. Mater.* **2016**, *1*, 16068. DOI
130. Zhang, J.; Yue, R.; Yang, K.; et al. Ion-exchange membranes based on framework materials for hydrogen-electrical energy interconversion. *Joule* **2026**, *10*, 102215. DOI
131. Sheng, F.; Ge, L.; Li, X.; Xu, T. Covalent organic framework membranes for selective ion separation. *Commun. Mater.* **2026**, *7*, 33. DOI
132. Li, W.; Li, Y.; Caro, J.; Huang, A. Fabrication of a flexible hydrogen-bonded organic framework based mixed matrix membrane for hydrogen separation. *J. Membr. Sci.* **2022**, *643*, 120021. DOI
133. Chen, C.; Shen, L.; Lin, H.; Zhao, D.; Li, B.; Chen, B. Hydrogen-bonded organic frameworks for membrane separation. *Chem. Soc. Rev.* **2024**, *53*, 2738-60. DOI
134. Wang, H.; Jiao, W. N.; Zhu, W. D.; et al. Stepwise post-modification of pyridine-imine COFs for enhanced hydrolytic stability and proton conductivity. *Angew. Chem.* **2025**, *137*, e202511559. DOI
135. Huang, Z.; Yi, J.; Xing, Z.; et al. Robust linkage-encoded covalent organic framework membranes sustain selective ion transport for energy harvesting from concentrated acids. *Angew. Chem. Int. Ed.* **2026**, *65*, e5918512. DOI
136. Yin, Q.; Alexandrov, E. V.; Si, D. H.; et al. Metallization-prompted robust porphyrin-based hydrogen-bonded organic frameworks for photocatalytic CO_2 reduction. *Angew. Chem. Int. Ed.* **2022**, *134*, e202115854. DOI
137. Kang, Z.; Guo, H.; Fan, L.; et al. Scalable crystalline porous membranes: current state and perspectives. *Chem. Soc. Rev.* **2021**, *50*, 1913-44. DOI
138. Yang, L.; Cao, L. N.; Li, S.; et al. MOFs/MXene nano-hierarchical porous structures for efficient ion dynamics. *Nano. Energy.* **2024**, *129*, 110076. DOI
139. Chhowalla, M. Editor's choice: advancements in nanoconfined materials for osmotic power generation. *MRS. Energy. Sustain.* **2024**, *11*, 192. DOI
140. Dou, H.; Xu, M.; Wang, B.; et al. Microporous framework membranes for precise molecule/ion separations. *Chem. Soc. Rev.* **2021**, *50*, 986-1029. DOI
141. Yang, R.; Fan, Y.; Mei, L.; et al. Synthesis of atomically thin sheets by the intercalation-based exfoliation of layered materials. *Nat. Synth.* **2023**, *2*, 101-18. DOI
142. Jian, M.; Qiu, R.; Xia, Y.; et al. Ultrathin water-stable metal-organic framework membranes for ion separation. *Sci. Adv.* **2020**, *6*, eaay3998. DOI
143. Yin, Q.; Pang, K.; Feng, Y.; et al. Hydrogen-bonded organic frameworks in solution enables continuous and high-crystalline membranes. *Nat. Commun.* **2024**, *15*, 634. DOI
144. Yang, Q.; Kang, B.; Han, W.; et al. Aqueous-phase preparation of high-quality COF nanofiltration membranes for dye/salt separation. *J. Membr. Sci.* **2026**, *741*, 125070. DOI
145. Duan, J.; Wang, X.; Li, W.; et al. Solvent-resistant poly HOF membranes with well-defined nanostructures and high structural stability. *Nano. Res.* **2025**, *18*, 94907406. DOI

146. Feng, S.; Shang, Y.; Wang, Z.; et al. Inside cover: fabrication of a hydrogen-bonded organic framework membrane through solution processing for pressure-regulated gas separation. *Angew. Chem. Int. Ed.* **2020**, *59*, 3750. DOI
147. Dey, K.; Pal, M.; Rout, K. C.; et al. Selective molecular separation by interfacially crystallized covalent organic framework thin films. *J. Am. Chem. Soc.* **2017**, *139*, 13083-91. DOI
148. Jiang, W.; Zhou, J.; Zhong, X.; et al. Axial alignment of covalent organic framework membranes for giant osmotic energy harvesting. *Nat. Sustain.* **2025**, *8*, 446-55. DOI
149. Matsumoto, M.; Valentino, L.; Stiehl, G. M.; et al. Lewis-acid-catalyzed interfacial polymerization of covalent organic framework films. *Chem* **2018**, *4*, 308-17. DOI
150. Ji, Y.; Gu, B.; Huo, H.; et al. Roll-to-roll fabrication of large-area metal-organic framework-based membranes for high-performance aqueous separations. *Nat. Water.* **2024**, *2*, 183-92. DOI
151. Li, Y.; Wee, L. H.; Volodin, A.; Martens, J. A.; Vankelecom, I. F. J. Polymer supported ZIF-8 membranes prepared via an interfacial synthesis method. *Chem. Commun.* **2015**, *51*, 918-20. DOI
152. Feng, Y.; Kang, Z.; Wang, Z.; et al. Preprocessed monomer interfacial polymerization for scalable fabrication of high-valent cluster-based metal-organic framework membranes. *J. Am. Chem. Soc.* **2024**, *146*, 33452-60. DOI
153. Yue, L.; Kong, F.; Wang, Y.; Sun, G.; Zhou, A.; Chen, J. Evolution of morphology, structure, and performance of the COF membranes with monomer concentrations: Enabling effective desalination and kinetics analysis. *Desalination* **2024**, *583*, 117712. DOI
154. Pan, Y.; Yu, G.; Gao, L.; et al. Ultra-rapid preparation of large-area high-crystallinity covalent organic framework membranes. *Nat. Commun.* **2025**, *17*, 857. DOI
155. Liu, Y.; Ng, Z.; Khan, E. A.; Jeong, H.; Ching, C.; Lai, Z. Synthesis of continuous MOF-5 membranes on porous α-alumina substrates. *Microporous. Mesoporous. Mater.* **2009**, *118*, 296-301. DOI
156. Fan, H.; Gu, J.; Meng, H.; Knebel, A.; Caro, J. High-flux membranes based on the covalent organic framework COF-LZU1 for selective dye separation by nanofiltration. *Angew. Chem. Int. Ed.* **2018**, *57*, 4083-7. DOI
157. Cheng, Y.; Datta, S. J.; Zhou, S.; Jia, J.; Shekhah, O.; Eddaoudi, M. Advances in metal-organic framework-based membranes. *Chem. Soc. Rev.* **2022**, *51*, 8300-50. DOI
158. Zhang, Z.; Jiao, J.; Jiang, Y.; et al. Defect engineering strategy of *in-situ* grown COF-300 nanofiltration membranes for selective dye separation. *J. Membr. Sci.* **2026**, *742*, 125166. DOI
159. Nunes, S. P.; Culfaz-emecen, P. Z.; Ramon, G. Z.; et al. Thinking the future of membranes: Perspectives for advanced and new membrane materials and manufacturing processes. *J. Membr. Sci.* **2020**, *598*, 117761. DOI
160. Pu, Y.; Zhao, M.; Liang, X.; et al. Growing ZIF-8 seeds on charged COF substrates toward efficient propylene-propane separation membranes. *Angew. Chem. Int. Ed.* **2023**, *62*, e202302355. DOI
161. Zhai, M.; Moghadam, F.; Gosiamemang, T.; Heng, J. Y. Y.; Li, K. Facile orientation control of MOF-303 hollow fiber membranes by a dual-source seeding method. *Nat. Commun.* **2024**, *15*, 10264. DOI
162. Chowdhury, M. R.; Steffes, J.; Huey, B. D.; Mccutcheon, J. R. 3D printed polyamide membranes for desalination. *Science* **2018**, *361*, 682-6. DOI
163. Yuan, K.; Song, T.; Yang, C.; et al. Polymer-assisted space-confined strategy for the foot-scale synthesis of flexible metal-organic framework-based composite films. *J. Am. Chem. Soc.* **2021**, *143*, 17526-34. DOI
164. Liu, K.; Qi, H.; Dong, R.; et al. On-water surface synthesis of crystalline, few-layer two-dimensional polymers assisted by surfactant monolayers. *Nature. Chem.* **2019**, *11*, 994-1000. DOI
165. Noh, J.; Jeong, S.; Lee, J. Ultrafast formation of air-processable and high-quality polymer films on an aqueous substrate. *Nat. Commun.* **2016**, *7*, 12374. DOI
166. Zhang, E.; Ding, S.; Feng, G.; et al. Chiral covalent organic framework for highly efficient spin polarization. *J. Am. Chem. Soc.* **2026**, *148*, 21305-12. DOI
167. Paul, S.; Pearson, C.; Molloy, A.; et al. Langmuir-Blodgett film deposition of metallic nanoparticles and their application to electronic memory structures. *Nano. Lett.* **2003**, *3*, 533-6. DOI
168. Chokprasombat, K.; Sirisathitkul, C.; Ratphonsan, P. Liquid-air interface self-assembly: a facile method to fabricate long-range nanoparticle monolayers. *Surf. Sci.* **2014**, *621*, 162-7. DOI
169. Fang, C.; Yoon, I.; Hubble, D.; Tran, T.; Kostecki, R.; Liu, G. Recent applications of Langmuir-Blodgett technique in battery research. *ACS. Appl. Mater. Interfaces.* **2022**, *14*, 2431-9. DOI
170. Zong, J.; Ma, W.; Jiang, Y.; et al. Giant osmotic power density generation with an anion-selective AB-stacking covalent-organic framework bilayer. *Innovation* **2025**, *6*, 100908. DOI
171. Makiura, R.; Motoyama, S.; Umemura, Y.; Yamanaka, H.; Sakata, O.; Kitagawa, H. Surface nano-architecture of a metal-organic framework. *Nat. Mater.* **2010**, *9*, 565-71. DOI

172. Gu, W.; Li, Q.; Wang, R.; Zhang, L.; Liu, Z.; Jiao, T. Recent progress in the applications of Langmuir-Blodgett film technology. *Nanomaterials* **2024**, *14*, 1039. DOI
173. Lu, G.; Shang, W.; Ma, X.; et al. Supramolecular nanocrystalline membranes with well-aligned subnanochannels for enhanced reverse osmosis desalination. *Nat. Commun.* **2025**, *16*, 6289. DOI
174. Mao, K.; Liu, C.; Ni, A.; et al. Optimization of ion transport in two-dimensional nanofluidic membranes for osmotic energy conversion. *Mater. Today.* **2025**, *82*, 274-88. DOI
175. Xiao, K.; Yang, T.; Liang, J.; et al. Nanofluidic voidless electrode for electrochemical capacitance enhancement in gel electrolyte. *Nat. Commun.* **2021**, *12*, 5515. DOI
176. Wang, F.; Zhang, Z.; Shakir, I.; Yu, C.; Xu, Y. 2D Polymer nanosheets for membrane separation. *Adv. Sci.* **2022**, *9*, 2103814. DOI
177. Rao, A. K.; Bolorinos, J.; Musabandesu, E.; Chapin, F. T.; Mauter, M. S. Valuing energy flexibility from water systems. *Nat. Water.* **2024**, *2*, 1028-37. DOI
178. Abdullah, N.; Yusof, N.; Ismail, A.; Lau, W. Insights into metal-organic frameworks-integrated membranes for desalination process: a review. *Desalination* **2021**, *500*, 114867. DOI
179. Tripathy, D. B. Recent advances on 2D metal organic framework (MOF) membrane for waste water treatment and desalination. *Desalination* **2024**, *592*, 118183. DOI
180. Zhao, S.; Jiang, C.; Fan, J.; et al. Hydrophilicity gradient in covalent organic frameworks for membrane distillation. *Nat. Mater.* **2021**, *20*, 1551-8. DOI
181. Gravelle, S.; Joly, L.; Detcheverry, F.; Ybert, C.; Cottin-Bizonne, C.; Bocquet, L. Optimizing water permeability through the hourglass shape of aquaporins. *Proc. Natl. Acad. Sci. U.S.A.* **2013**, *110*, 16367-72. DOI
182. Wei, X.; Liu, Y.; Zhao, F.; et al. Covalent organic framework membrane with hourglass-shaped nanochannels for ultrafast desalination. *Nat. Commun.* **2025**, *16*, 8125. DOI
183. Xiao, K.; Jiang, L.; Antonietti, M. Ion transport in nanofluidic devices for energy harvesting. *Joule* **2019**, *3*, 2364-80. DOI
184. Wang, P.; Tao, W.; Zhou, T.; et al. Nanoarchitectonics in advanced membranes for enhanced osmotic energy harvesting. *Adv. Mater.* **2024**, *36*, 2404418. DOI
185. Lin, W.; Huang, T.; Bai, C.; et al. Novel ultrastable 2D MOF/MXene nanofluidic membrane with ultralow resistance for highly efficient osmotic power harvesting. *Nano. Energy.* **2024**, *128*, 109924. DOI
186. Xie, B.; Xiong, T.; Li, W.; et al. Perspective on nanofluidic memristors: from mechanism to application. *Chem-Asian. J.* **2022**, *17*, e202200682. DOI
187. Zhang, M.; Xu, G.; Zhang, H.; Xiao, K. Nanofluidic volatile threshold switching ionic memristor: a perspective. *ACS. Nano.* **2025**, *19*, 10589-98. DOI
188. Xu, G.; Zhang, M.; Mei, T.; Liu, W.; Wang, L.; Xiao, K. Nanofluidic ionic memristors. *ACS. Nano.* **2024**, acsnano.4c06467. DOI
189. Zhang, P.; Xia, M.; Zhuge, F.; et al. Nanochannel-based transport in an interfacial memristor can emulate the analog weight modulation of synapses. *Nano. Lett.* **2019**, *19*, 4279-86. DOI
190. Yu, S.; Hu, J.; Li, Z.; et al. Metal-organic framework nanofluidic synapse. *J. Am. Chem. Soc.* **2024**, *146*, 27022-9. DOI
191. Sun, P. Z.; Yang, Q.; Kuang, W. J.; et al. Limits on gas impermeability of graphene. *Nature* **2020**, *579*, 229-32. DOI
192. Wahab, O. J.; Daviddi, E.; Xin, B.; et al. Proton transport through nanoscale corrugations in two-dimensional crystals. *Nature* **2023**, *620*, 782-6. DOI
193. Casciola, M.; Alberti, G.; Sganappa, M.; Narducci, R. On the decay of Nafion proton conductivity at high temperature and relative humidity. *J. Power. Sources.* **2006**, *162*, 141-5. DOI
194. Sun, P. Z.; Yagmurcukardes, M.; Zhang, R.; et al. Exponentially selective molecular sieving through angstrom pores. *Nat. Commun.* **2021**, *12*, 7170. DOI
195. Wu, Z. F.; Sun, P. Z.; Wahab, O. J.; et al. Proton and molecular permeation through the basal plane of monolayer graphene oxide. *Nat. Commun.* **2023**, *14*, 7756. DOI
196. Mogg, L.; Hao, G.; Zhang, S.; et al. Atomically thin micas as proton-conducting membranes. *Nat. Nanotechnol.* **2019**, *14*, 962-6. DOI
197. Ji, Y.; Hao, G.; Tan, Y.; et al. High proton conductivity through angstrom-porous titania. *Nat. Commun.* **2024**, *15*, 10546. DOI
198. Zhu, L.; Yang, H.; Xu, T.; Shen, F.; Si, C. Precision-engineered construction of proton-conducting metal-organic frameworks. *Nano-Micro. Lett.* **2024**, *17*, 87. DOI
199. Kidambi, P. R.; Chaturvedi, P.; Moehring, N. K. Subatomic species transport through atomically thin membranes: present and future applications. *Science* **2021**, *374*, eabd7687. DOI
200. Dasgupta, S.; Saha, S.; Paesani, F. Sub-nanometer confinement suppresses autoionization of water. *J. Am. Chem. Soc.* **2025**, *147*, 25167-73. DOI
201. Wang, R.; Souilamas, M.; Esfandiar, A.; et al. In-plane dielectric constant and conductivity of confined water. *Nature* **2025**, *646*, 606-10. DOI

202. Shimizu, G. K. H.; Taylor, J. M.; Kim, S. Proton conduction with metal-organic frameworks. *Science* **2013**, *341*, 354-5. DOI
203. Lim, D.; Kitagawa, H. Proton transport in metal-organic frameworks. *Chem. Rev.* **2020**, *120*, 8416-67. DOI
204. Shi, B.; Pang, X.; Li, S.; et al. Short hydrogen-bond network confined on COF surfaces enables ultrahigh proton conductivity. *Nat. Commun.* **2022**, *13*, 6666. DOI
205. Fang, R.; Han, Z.; Li, J.; et al. Rationalized design of hyperbranched trans-scale graphene arrays for enduring high-energy lithium metal batteries. *Sci. Adv.* **2022**, *8*, eadc9961. DOI
206. Hong, Z.; Yuan, H.; Wu, H.; et al. 2D Vertically conductive metal-organic framework electrolytes: will they outperform 3D MOFs for solid state batteries? *Small* **2025**, *21*, 2408394. DOI
207. Song, C.; Pan, L.; Wu, J.; et al. Bioinspired interfacial nanofluidic layer enabling high-rate and dendrite-free lithium metal negative electrodes. *Nat. Commun.* **2025**, *16*, 8056. DOI
208. Bai, S.; Liu, X.; Zhu, K.; Wu, S.; Zhou, H. Metal-organic framework-based separator for lithium-sulfur batteries. *Nat. Energy.* **2016**, *1*, 16094. DOI
209. Song, C.; Pan, L.; Chen, L.; et al. Nanofluidic-enhanced high-mass-loading electrodes for energy-dense and high-rate lithium-sulfur batteries. *Energy. Environ. Sci.* **2025**, *18*, 8244-55. DOI
210. Emmerich, T.; Ronceray, N.; Agrawal, K. V.; et al. Nanofluidics. *Nat. Rev. Methods. Primers.* **2024**, *4*, 69. DOI
211. Tian, Y.; Song, Y.; Xia, Y.; et al. Nanoscale one-dimensional close packing of interfacial alkali ions driven by water-mediated attraction. *Nat. Nanotechnol.* **2023**, *19*, 479-84. DOI
212. Wang, B.; Fang, Z.; Jiang, Q.; et al. Interlayer confined water enabled pseudocapacitive sodium-ion storage in nonaqueous electrolyte. *ACS. Nano.* **2024**, *18*, 798-808. DOI
213. Ge, K.; Shao, H.; Lin, Z.; Taberna, P.; Simon, P. Advanced characterization of confined electrochemical interfaces in electrochemical capacitors. *Nat. Nanotechnol.* **2025**, *20*, 196-208. DOI
214. Smirnov, S. N.; Vlassiouk, I. V.; Lavrik, N. V. Voltage-gated hydrophobic nanopores. *ACS. Nano.* **2011**, *5*, 7453-61. DOI
215. Haigh, S. J.; Gholinia, A.; Jalil, R.; et al. Cross-sectional imaging of individual layers and buried interfaces of graphene-based heterostructures and superlattices. *Nat. Mater.* **2012**, *11*, 764-7. DOI
216. Zou, K.; Ling, H.; Wang, Q.; et al. Turing-type nanochannel membranes with extrinsic ion transport pathways for high-efficiency osmotic energy harvesting. *Nat. Commun.* **2024**, *15*, 10231. DOI
217. Comtet, J.; Grosjean, B.; Glushkov, E.; et al. Direct observation of water-mediated single-proton transport between hBN surface defects. *Nat. Nanotechnol.* **2020**, *15*, 598-604. DOI
218. Hou, Y.; Hou, X. Bioinspired nanofluidic iontronics. *Science* **2021**, *373*, 628-9. DOI
219. Kumar, M.; Stone, H. A. Membrane science emerging as a convergent scientific field with molecular origins and understanding, and global impact. *Proc. Natl. Acad. Sci. U.S.A.* **2021**, *118*, e2106494118. DOI